adapted version of DNMR3.[46] NMR probe temperatures were calibrated by using the method of van Geet[47] and are considered accurate to ±2 K.

$^{13}C\{^1H\}$ EXSY spectra were obtained with either broad-band or composite-pulse ^1H decoupling, using the Bruker automation microprogram NOESY ($D1$–$\pi/2$–$D0$–$\pi/2$–$D9$–$\pi/2$–FID–acquire). The data table was acquired by using 1024 words in the F_2 dimension and 256 words in the F_1 dimension zero-filled to 512. Spectral widths were typically 1 kHz, and recycle delays ($D1$) typically 4–6 s. The initial value of the incremented delay $D0$ was 3 μs. For the low-temperature experiments, a cycle of either 8 or 16 scans were acquired for each F_2 FID, with total acquisition times of ca. 4–8 h. A random variation of ±15% was applied to the mixing time delay t_m ($D9$) to reduce any correlations arising from scalar coupling. Apodization was applied to all data sets before Fourier transform, using either $\pi/6$ shifted sine-bell or exponential line-broadening (LB = 2) functions. EXSY spectra were symmetrized about the $F_1 = F_2$ diagonal. For complex **4** the volume integrals, corresponding to the diagonal and off-diagonal elements of the intensity matrix, were obtained by integration of the submatrix rows of the EXSY spectra containing the most intense peaks (usually six to ten rows). For complex **3** integrations were carried out both in the above manner and also by using the box-integral routine of the Bruker AP2D display program. Errors in the integrals were estimated from the integrated intensity of identical sized boxes in noise areas of the EXSY spectrum. There was satisfactory agreement between the derived rate data using either method. Individual exchange rate constants were obtained from the intensity matrix by using the program D2DNMR.[26]

Due to the possibility that apodization functions could adversely affect relative line widths, and hence relative intensities, the effect of using (a) no apodization, (b) $\pi/6$ shifted sine-bell, and (c) Lorentz–Gaussian line narrowing on the data for **3** at 225 K was examined. Apart from the rates associated with the b/c/e tripodal rotation, which appear ill-conditioned in this analysis, there were no serious discrepancies. Rates for the exchanges associated with the PtL_3 rotation varied from ca. 0.1 to 0.2 s^{-1}, which are within the range of the reported rate errors. The discrepancies seen for the b/c/e exchange rate constants (which must be regarded as unreliable at 225 K) are attributed to experimental errors arising from the broadness of the diagonal peaks and cross-peaks associated with this process, overlap of some ^{195}Pt satellites, and generally poor S/N ratios. In order to a ensure a reasonably constant temperature over the whole experiment, the low-temperature acquisitions were limited to a ca. 8-h time period, allowing only a maximum of 16 transients per $D0$ increment.

Acknowledgment. Dr. David Stephenson (Exeter) is thanked for a copy of the 2D EXSY kinetic analysis program D2DNMR and Johnson-Matthey for a generous loan of Pt salts.

Registry No. **3**, 112548-92-2; **4**, 112574-99-9.

(46) Kleier, D. A.; Binsch, G. *QCPE* **1970**, *11*, 165.
(47) van Geet, A. L. *Anal. Chem.* **1970**, *42*, 679.

Experimental, Structural, and Theoretical Studies of Diplatinum Complexes Containing Bridging Phenylethenylidene Ligands Including the Excited-State Chemistry and Photophysics of Photochemically Generated Species

Eduardo Baralt,[1a] Edward A. Boudreaux,*[,1b] James N. Demas,*[,1c] P. Galen Lenhert,*[,1d] C. M. Lukehart,*[,1a] Andrew T. McPhail,*[,1e] Donald R. McPhail,[1e] James B. Myers, Jr.,[1a] LouAnn Sacksteder,[1c] and William R. True[1a]

Departments of Chemistry at Vanderbilt University, Nashville, Tennessee 37235, University of New Orleans, New Orleans, Louisiana 70148, University of Virginia, Charlottesville, Virginia 22901, and Duke University, Durham, North Carolina 27706, and the Department of Physics and Astronomy, Vanderbilt University, Nashville, Tennessee 37235

Received May 1, 1989

The results of a comprehensive investigation of the chemistry of the diplatinum compound $[Pt_2(\mu\text{-}C{=}CHPh)(C{\equiv}CPh)(PEt_3)_4]BF_4$ (**1**) and related derivatives are presented. Complex **1** reacts with halides, NCS^-, and various RS^- nucleophiles to give the neutral compounds $[Pt_2(\mu\text{-}C{=}CHPh)(C{\equiv}CPh)(PEt_3)_3X]$ with loss of one PEt_3 ligand. These Pt_2X complexes react with acid and X^- nucleophile to give the neutral compounds $[Pt_2(\mu\text{-}C{=}CHPh)(PEt_3)_3X_2]$ upon loss of phenylacetylene. The X-ray structures of the Pt_2Cl, Pt_2I, and Pt_2Br_2 complexes have been determined. $[Pt_2(\mu\text{-}C{=}CHPh)(C{\equiv}CPh)(PEt_3)_3Cl]$: monoclinic; $P2_1/c$; $Z = 4$; $a = 11.685$ (1) Å, $b = 20.810$ (7) Å, $c = 19.172$ (4) Å; $\beta = 123.96$ (1)°. $[Pt_2(\mu\text{-}C{=}CHPh)(C{\equiv}CPh)(PEt_3)_3I]$: orthorhombic; $Pbca$; $Z = 8$; $a = 18.004$ (3) Å, $b = 22.805$ (4) Å, $c = 19.328$ (4) Å. $[Pt_2(\mu\text{-}C{=}CHPh)(PEt_3)_3Br_2]$: monoclinic; Cc; $Z = 8$; $a = 10.359$ (1) Å, $b = 33.054$ (9) Å, $c = 19.855$ (5) Å; $\beta = 93.40$ (2)°. SC-MEH-MO calculations of the electronic structure of compound **1** indicate a large negative charge on each of the Pt atoms which is reminiscent of the results reported earlier from similar calculations on the anion $Pt_2(P_2O_5H_2)_4^{4-}$. Similarities between the photochemistry of the complexes reported herein and that known for $Pt_2(P_2O_5H_2)_4^{4-}$ are presented. Complex **1** reacts with MeI under photolysis to give Pt_2I and Pt_2I_2, and it reacts as a catalyst under photolysis to produce acetone and molecular hydrogen from 2-propanol. The complex Pt_2Cl emits a red-orange luminescence at 696 nm in a 4:1 ethanol/methanol matrix at 77 K upon excitation at 410 nm. This luminescent state has an average lifetime of 1.7 μs and is attained with an "optical" quantum yield of 0.010 (2).

One of us has reported recently that the cationic diplatinum complex $[Pt_2(\mu\text{-}C{=}CHPh)(C{\equiv}CPh)(PEt_3)_4]BF_4$ (**1**), is formed readily by the addition of the Pt—H bond of $[HPt(PEt_3)_2(acetone)]BF_4$ across one of the C≡C triple

0276-7333/89/2308-2417$01.50/0

bonds of the dialkynyl complex [*trans*-Pt(C≡CPh)$_2$(PEt$_3$)$_2$].[2] Complex **1** can be isolated kinetically as isomer **1a**; however, under prolonged reaction time, compound **1a** slowly isomerizes to isomer **1b**.[3] The X-ray structure of

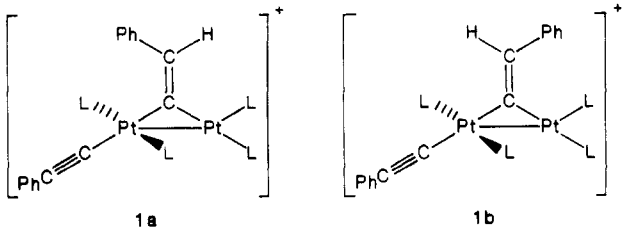

1a **1b**

1a has established the overall molecular structure and has revealed a Pt–Pt distance of 2.750 (2) Å.[2] The synthetic method utilized to prepare compound **1** has been extended to include the synthesis of several other diplatinum and heterodinuclear (Pt–M) complexes containing μ-alkenylidene ligands.[3] Similar additions of Pt—H or Pt—R bonds across the M≡C triple bonds of terminal alkylidyne ligands gives heterodinuclear (Pt—M) complexes containing μ-alkylidene ligands,[4] and Pt—H addition across the M=C double bond of a terminal phenylethenylidene ligand gives a heterodinuclear complex containing a bridging phenylethenyl ligand.[5]

Further development of this synthetic method for the preparation of dinuclear compounds containing bridging hydrocarbyl ligands would be justified if the products of these reactions exhibited interesting chemical behavior. To explore this possibility, we investigated the chemical reactivity of complex **1**. The results of this investigation are reported below. While complex **1** exhibits only limited thermal reactivity, it (and some of its derivatives) exhibits significant and unexpected photochemical reactivity. Theoretical calculations indicate a similarity between the electronic structure of the cationic, diplatinum complex **1a** and that of the tetrakis(μ-pyrophosphito)diplatinum anion $Pt_2(P_2O_5H_2)_4^{4-}$ ($Pt_2(POP)_4^{4-}$), even though these two complexes have quite different molecular structures. The photochemical reactivity of these two types of complexes is similar, also. Our preliminary results of a study of the electronic structure of **1a** and of the photochemistry of **1a** and some of its derivatives are also presented below.

Experimental Section

Materials and Methods. All reactions were preformed under dry, prepurified nitrogen. Solvent purification procedures, spectroscopic methods, microanalytical services, and reagent preparation procedures have been published previously.[2,3,5] Photochemical reactions conducted on a synthetic scale were effected by using either a 100-W, Hanovia medium-pressure mercury lamp and a Pyrex glass reaction vessel or a Rayonet preparative photochemical reactor (Model RPR-208) and RPR-3500 Å lamps in a Pyrex glass reaction vessel fitted with a cold finger to maintain a reaction temperature of 16 °C.

Preparation of [Pt$_2$(μ-C=CHPh)(C≡CPh)(PEt$_3$)$_3$Cl] (2). To a stirred solution of 0.17 mmol of **1b** in 25 mL of THF was added 0.20 mmol of LiCl. The reaction solution was stirred at 25 °C for 14 h. The solvent was removed at reduced pressure, and the orange residue was extracted with 3 × 10 mL of diethyl ether. The extracts were filtered through neutral alumina in a Schlenk frit. The solvent was removed from the filtrate in vacuo, and the resulting orange powder was crystallized from THF/hexane (1:5 v/v) at −15 °C. Complex **2** was isolated as orange-red crystals (63%): mp 146–148 °C; IR (hexane) ν(C≡C) 2115 (w) cm^{-1}; ^{1}H NMR ($CDCl_3$) δ 1.17 (m, 27, CH_3), 2.00 (m, 12, CH_2), 2.40 (m, 6, CH_2), 6.80 (d, 1, CHPh, $^4J_{^{31}P-^1H}$ = 17.5 Hz), 7.00–7.45 (complex m, 8, 1 3/5 Ph), 7.77 (d, 2, ortho Ph, J = 7.43 Hz); $^{31}P\{^1H\}$ NMR (5% $CDCl_3/CHCl_3$) δ 27.2 (s, 1, PEt_3, $^1J_{^{195}Pt-^{31}P}$ = 5672 Hz, $^2J_{^{195}Pt-^{31}P}$ = 414 Hz), 13.7 (s, 2, trans PEt_3, $^1J_{^{195}Pt-^{31}P}$ = 2215 Hz, $^2J_{^{195}Pt-^{31}P}$ = 40.1 Hz). Anal. Calcd for $C_{34}H_{56}ClP_3Pt_2$: C, 41.53; H, 5.73; P, 9.45. Found: C, 41.22; H, 5.66; P, 9.82.

Preparation of [Pt$_2$(μ-C=CHPh)(C≡CPh)(PEt$_3$)$_3$Br] (3). To a stirred solution of 0.13 mmol of **1b** in 20 mL of THF was added 0.15 mmol of LiBr. The reaction solution was stirred at 25 °C for 3 h. The solvent was removed at reduced pressure, and the orange residue was extracted with 3 × 10 mL of diethyl ether. The extracts were filtered through neutral alumina in a Schlenk frit. The solvent was removed from the filtrate in vacuo, and the resulting orange powder was crystallized from THF/hexane (1:4 v/v) at −15 °C. Complex **3** was isolated as orange-red crystals (72%): mp 143–145 °C; IR (hexane) ν(C≡C) 2115 (w) cm^{-1}; ^{1}H NMR ($CDCl_3$) δ 1.15 (m, 27, CH_3), 1.95 (m, 6, CH_2), 2.05 (m, 6, CH_2), 2.42 (m, 6, CH_2), 6.80 (d, 1, CHPh, $^4J_{^{31}P-^1H}$ = 18.3 Hz), 7.05–7.35 (complex m, 8, 1 3/5 Ph), 7.85 (d, 2, ortho Ph, J = 7.43 Hz); $^{31}P\{^1H\}$ NMR (5% $CDCl_3/CHCl_3$) δ 28.2 (s, 1, PEt_3, $^1J_{^{195}Pt-^{31}P}$ = 5644 Hz, $^2J_{^{195}Pt-^{31}P}$ = 399 Hz), 13.4 (s, 2, trans PEt_3, $^1J_{^{195}Pt-^{31}P}$ = 2212 Hz, $^2J_{^{195}Pt-^{31}P}$ = 52.8 Hz). Anal. Calcd for $C_{34}H_{56}BrP_3Pt_2$: C, 39.73; H, 5.49; Br, 7.78; P, 9.04. Found: C, 39.91; H, 5.49; Br, 7.88; P, 8.83.

Preparation of [Pt$_2$(μ-C=CHPh)(C≡CPh)(PEt$_3$)$_3$I] (4). To a stirred solution of 0.13 mmol of **1b** in 20 mL of THF was added 0.16 mmol of NaI. The reaction solution was stirred at 25 °C for 2 h. The solvent was removed at reduced pressure, and the red residue was extracted with 3 × 10 mL of diethyl ether. The extracts were filtered through neutral alumina in a Schlenk frit. The solvent was removed from the filtrate in vacuo, and the resulting red-orange powder was crystallized from THF/hexane (1:7 v/v) at −15 °C. Complex **4** was isolated as red crystals (65%): mp 151–153 °C; IR (hexane) ν(C≡C) 2115 (w) cm^{-1}; ^{1}H NMR ($CDCl_3$) δ 1.15 (m, 27, CH_3), 1.95 (m, 6, CH_2), 2.05 (m, 6, CH_2), 2.40 (m, 6, CH_2), 6.75 (d, 1, CHPh, $^4J_{^{31}P-^1H}$ = 19.4 Hz), 7.00–7.35 (complex m, 8, 1 3/5 Ph), 7.85 (d, 2, ortho Ph, J = 7.40 Hz); $^{31}P\{^1H\}$ NMR (5% $CDCl_3/CHCl_3$) δ 31.3 (s, 1, PEt_3, $^1J_{^{195}Pt-^{31}P}$ = 5599 Hz, $^2J_{^{195}Pt-^{31}P}$ = 376 Hz), 12.4 (s, 2, trans PEt_3, $^1J_{^{195}Pt-^{31}P}$ = 2212 Hz, $^2J_{^{195}Pt-^{31}P}$ = 36.6 Hz). Anal. Calcd for $C_{34}H_{56}IP_3Pt_2$: C, 38.00; H, 5.25; I, 11.81; P, 8.64. Found: C, 37.73; H, 4.97; I, 11.69; P, 8.79.

Preparation of [Pt$_2$(μ-C=CHPh)(C≡CPh)(PEt$_3$)$_3$(NCS)] (5). To a stirred solution of 0.13 mmol of **1b** in 20 mL of THF was added 0.15 mmol of KNCS. The reaction solution was stirred at 25 °C for 3 h. The solvent was removed at reduced pressure, and the orange residue was extracted with 3 × 15 mL of diethyl ether. The extracts were filtered through neutral alumina in a Schlenk frit. The solvent was removed from the filtrate in vacuo, and the resulting orange powder was crystallized from THF/hexane (1:4 v/v) at −15 °C. Complex **5** was isolated as red-orange crystals (54%): mp 156–157 °C; IR (hexane) ν(CN) 2085 (vs) cm^{-1}; ^{1}H NMR ($CDCl_3$) δ 1.18 (m, 27, CH_3), 1.97 (m, 12, CH_2), 2.31 (m, 6, CH_2), {6.76 [d, 0.63, CHPh (–N=C=S isomer), $^4J_{^{31}P-^1H}$ = 18.15 Hz], 6.95 [d, 0.37, CHPh (–S—C≡N isomer), $^4J_{^{31}P-^1H}$ = 18.15 Hz]}, 7.00–7.40 (complex m, 8, 1 3/5 Ph), {7.75 [d, 1.26, ortho Ph (–N=C=S isomer), J = 7.30 Hz], 7.78 [d, 0.74, ortho Ph (–S—C≡N isomer), J = 7.45 Hz]}; $^{31}P\{^1H\}$ NMR (5% $CDCl_3/CHCl_3$) δ 25.8 (s, PEt_3 (–N=C=S isomer), $^1J_{^{195}Pt-^{31}P}$ = 5372 Hz, $^2J_{^{195}Pt-^{31}P}$ = 419 Hz), 25.7 (s, PEt_3(–S—C≡N isomer), $^1J_{^{195}Pt-^{31}P}$ = 5434 Hz, $^2J_{^{195}Pt-^{31}P}$ = 398 Hz), 15.6 (s, trans PEt_3 (–N=C=S isomer), $^1J_{^{195}Pt-^{31}P}$ = 2194 Hz, $^2J_{^{195}Pt-^{31}P}$ = 42.3 Hz), 14.2 (s, trans PEt_3 (–S—C≡N isomer), $^1J_{^{195}Pt-^{31}P}$ =2184 Hz, $^2J_{^{195}Pt-^{31}P}$ = 36.8 Hz). Anal. Calcd for $C_{35}H_{56}NP_3Pt_2S$: C, 41.71; H, 5.60; P, 9.22. Found: C, 41.28; H, 5.43; P, 9.30.

(1) (a) Department of Chemistry, Vanderbilt University. (b) Department of Chemistry, University of New Orleans. (c) Department of Chemistry, University of Virginia. (d) Department of Physics and Astronomy, Vanderbilt University. (e) Department of Chemistry, Duke University.

(2) Afzal, D.; Lenhert, P. G.; Lukehart, C. M. *J. Am. Chem. Soc.* **1984**, *106*, 3050–3052.

(3) Afzal, D.; Lukehart, C. M. *Organometallics* **1987**, *6*, 546–550.

(4) (a) Davis, J. H., Jr.; Lukehart, C. M. *Organometallics* **1984**, *3*, 1763–1764. (b) Davis, J. H., Jr.; Lenhert, P. G.; Lukehart, C. M.; Sacksteder, L. A. *Acta Crystallogr., Sect. C* **1986**, *C42*, 1133–1136. (c) Davis, J. H., Jr.; Lukehart, C. M.; Sacksteder, L. A. *Organometallics* **1987**, *6*, 50–55.

(5) Lukehart, C. M.; True, W. R. *Organometallics* **1988**, *7*, 2387–2393.

Preparation of $[Pt_2(\mu\text{-}C{=}CHPh)(C{\equiv}CPh)(PEt_3)_3(SPh)]$ (6). A THF solution of lithium thiophenolate was prepared as follows. A stirred solution of 0.24 mmol of *n*-BuLi in 5 mL of THF was cooled to 0 °C. Thiophenol (0.24 mmol) was added to this solution dropwise, and the solution was allowed to stir for 10 min.

To a stirred solution of 0.22 mmol of **1b** in 20 mL of THF was added the solution containing 0.24 mmol of lithium thiophenolate. An immediate color change from red to dark purple-red was observed. The reaction solution was stirred at 25 °C for 1 h. The solvent was removed at reduced pressure, and the deep red residue was extracted with 2 × 15 mL of diethyl ether. The extracts were filtered through neutral alumina in a Schlenk frit. The solvent was removed from the filtrate in vacuo, and the resulting red oil was chromatographed on a neutral alumina column (18 mm × 180 mm), using hexane as the eluting solvent. A single dark-red band was collected, and the product was crystallized from THF/hexane (1:9 v/v) at −15 °C. Complex **6** was isolated as dark purple crystalline blocks (75%): mp 77–79 °C; IR (hexane) ν(C≡C) 2110 (w) cm^{-1}, ^1H NMR ($CDCl_3$) δ 1.13 (m, 27, CH_3), 1.96 (m, 12, CH_2), 2.34 (m, 6, CH_2), 6.82 (t, 1.0, para Ph–S), 7.05–7.40 (complex m, 11, 1 3/5 Ph + 2/5 Ph–S + CHPh), 7.64 (d, 2.0, ortho Ph–S, J = 7.30 Hz), 7.86 (d, 2.0, ortho Ph, J = 7.65 Hz); $^{31}P\{^1H\}$ NMR (5% $CDCl_3/CHCl_3$) δ 27.7 (s, 1, PEt_3, $^1J_{^{195}Pt-^{31}P}$ = 5586 Hz, $^2J_{^{195}Pt-^{31}P}$ = 400 Hz), 11.6 (s, 2, trans PEt_3, $^1J_{^{195}Pt-^{31}P}$ = 2244 Hz, $^2J_{^{195}Pt-^{31}P}$ = 34.9 Hz). Anal. Calcd for $C_{40}H_{61}P_3Pt_2S$: C, 45.45; H, 5.81; P, 8.79; S, 3.03. Found: C, 45.62; H, 5.87; P, 8.96; S, 3.27.

Preparation of $[Pt_2(\mu\text{-}C{=}CHPh)(C{\equiv}CPh)(PEt_3)_3(SCHMe_2)]$ (7). A THF solution of lithium isopropylthiolate was prepared as follows. A stirred solution of 0.11 mmol of *n*-BuLi in 5 mL of THF was cooled to 0 °C. Isopropyl mercaptan (0.11 mmol) was added to this solution dropwise, and the solution was allowed to stir for 10 min.

To a stirred solution of 0.11 mmol of **1b** in 20 mL of THF was added the solution containing 0.11 mmol of lithium isopropylthiolate. An immediate color change from red to bright orange-yellow was observed. The reaction solution was stirred at 25 °C for 2 h. The solvent was removed at reduced pressure, and the yellow residue was extracted with 2 × 15 mL of diethyl ether. The extracts were filtered through neutral alumina in a Schlenk frit. The solvent was removed from the filtrate in vacuo, and the resulting yellow solid was chromatographed on a neutral alumina column (18 mm × 180 mm), using 20% ether/hexane as the eluting solvent. A single bright yellow band was collected, and the product was crystallized from THF/hexane (1:6 v/v) at −15 °C. Complex **7** was isolated as a bright yellow solid (62%): mp 152–154 °C; IR (hexane) ν(C≡C) 2115 (w) cm^{-1}; ^1H NMR ($CDCl_3$) δ 1.10 (m, 6, $CH(CH_3)_2$), 1.15 (m, 27, CH_3), 1.45 (m, 1, CH), 1.65 (m, 6, CH_2), 1.85 (m, 6, CH_2), 2.15 (m, 6, CH_2), 7.00–7.45 (complex m, 9, 1 3/5 Ph + CHPh), 7.90 (d, 2, ortho Ph, J = 7.45 Hz). Anal. Calcd for $C_{37}H_{63}P_3Pt_2S$: C, 43.44; H, 6.20; P, 9.08. Found: C, 43.70; H, 6.18; P, 9.91.

Preparation of $[Pt_2(\mu\text{-}C{=}CHPh)(C{\equiv}CPh)(PEt_3)_3(SC_6Cl_5)]$ (8). To a stirred solution of 0.14 mmol of **1b** in 20 mL of THF was added 0.15 mmol of $NaSC_6Cl_5$. The reaction solution was stirred at 25 °C for 2 h. The solvent was removed at reduced pressure, and the orange-red residue was extracted with 3 × 10 mL of diethyl ether. The extracts were filtered through neutral alumina in a Schlenk frit. The solvent was removed from the filtrate in vacuo, and the residue was chromatographed on a neutral alumina column (18 mm × 180 mm), using 10% ether/hexane as the eluting solvent. Complex **8** was isolated as a red-orange oil (71%): IR (hexane) ν(C≡C) 2110 (w) cm^{-1}; ^1H NMR ($CDCl_3$) δ 1.10 (m, 27, CH_3), 1.65 (m, 6, CH_2), 2.05 (m, 6, CH_2), 2.45 (m, 6, CH_2), 6.85 (d, 1, CHPh, $^4J_{^{31}P-^1H}$ = 18.48 Hz), 7.00–7.40 (complex m, 8, 1 3/5 Ph), 7.80 (d, 2, ortho Ph, J = 7.30 Hz); $^{31}P\{^1H\}$ NMR (5% $CDCl_3/CHCl_3$) δ 23.0 (s, 1, PEt_3, $^1J_{^{195}Pt-^{31}P}$ = 5613 Hz, $^2J_{^{195}Pt-^{31}P}$ = 388 Hz), 12.5 (s, 2, trans PEt_3, $^1J_{^{195}Pt-^{31}P}$ = 2195 Hz, $^2J_{^{195}Pt-^{31}P}$ = 36.0 Hz).

Preparation of $[Pt_2(\mu\text{-}C{=}CHPh)(PEt_3)_3Cl_2]$ (9). To a stirred solution of 0.10 mmol of compound **2** in 10 mL of diethyl ether was added 0.10 mL of a 1.54 M solution of HCl in diethyl ether. After 6 h, the solution changed color from orange-red to pale orange. The solution was filtered through neutral alumina in a Schlenk frit. The solvent was removed at reduced pressure. The pale orange residue was crystallized from CH_2Cl_2/n-hexane (1:6 v/v) at −15 °C. Complex **9** was isolated as orange crystals (65%): mp 168–169 °C; ^1H NMR (CD_2Cl_2) δ 1.10 (m, 27, CH_3), 1.84 (m, 6, CH^A_2), 1.96 (m, 6, CH_2), 2.25 (m, 6, CH^B_2), 6.11 (d, 1, CHPh, $^3J_{^{195}Pt-^1H}$ = 43 Hz, $^4J_{^{31}P-^1H}$ = 12.9 Hz), 7.05 ("t", 1, para Ph), 7.14 (t, 2, meta Ph, J = 7.01 Hz), 7.89 (d, 2, ortho Ph, J = 8.76 Hz); $^{31}P\{^1H\}$ NMR (5% $CDCl_3/CHCl_3$) δ 14.87 (s, 2, trans PEt_3, $^1J_{^{195}Pt-^{31}P}$ = 2311 Hz, $^2J_{^{195}Pt-^{31}P}$ = 51.2 Hz), 20.70 (s, 1, PEt_3, $^1J_{^{195}Pt-^{31}P}$ = 5481 Hz, $^2J_{^{195}Pt-^{31}P}$ = 614 Hz). Anal. Calcd for $C_{26}H_{51}P_3Pt_2Cl_2$: C, 34.03; H, 5.60; P, 10.13; Cl, 7.73. Found: C, 34.22; H, 5.86; P, 10.43; Cl, 7.59.

Preparation of $[Pt_2(\mu\text{-}C{=}CHPh)(PEt_3)_3Br_2]$ (10). To a stirred solution of 0.10 mmol of compound **3** in 10 mL of diethyl ether was added 0.10 mL of a 1.53 M solution of HBr in diethyl ether. The reaction solution was stirred at 25 °C for 6 h. The solution changed color from orange-red to pale orange. The solution was filtered through neutral alumina in a Schlenk frit. The solvent was removed from the filtrate in vacuo, and the resulting powder was crystallized from CH_2Cl_2/n-hexane (1:6 v/v) at −15 °C. Complex **10** was isolated as pale orange crystals (76%): mp 180–185 °C; ^1H NMR (CD_2Cl_2) δ 1.10 (m, 27, CH_3), 1.93 (m, 12, CH_2), 2.30 (m, 6, CH_2), 6.10 (d, 1, CHPh, $^3J_{^{195}Pt-^1H}$ = 57 Hz), $^4J_{^{31}P-^1H}$ = 8.4 Hz), 7.06 (d, 1, para Ph, J = 6.51 Hz), 7.12 ("t", 2, meta Ph, J = 6.19 Hz), 7.90 (d, 2, ortho Ph, J = 7.1 Hz); $^{31}P\{^1H\}$ NMR (5% $CDCl_3/CHCl_3$) δ 13.80 (s, 2, trans PEt_3, $^1J_{^{195}Pt-^{31}P}$ = 2281 Hz, $^2J_{^{195}Pt-^{31}P}$ = 47.0 Hz), 20.73 (s, 1, PEt_3, $^1J_{^{195}Pt-^{31}P}$ = 5426 Hz, $^2J_{^{195}Pt-^{31}P}$ = 603 Hz). Anal. Calcd for $C_{26}H_{51}P_3Pt_2Br_2$: C, 31.02, H, 5.11, P, 9.23. Found: C, 31.35; H, 5.23; P, 8.97.

Preparation of $[Pt_2(\mu\text{-}C{=}CHPh)(PEt_3)_3I_2]$ (11). To a stirred solution of 0.10 mmol of compound **4** in 10 mL of diethyl ether was added 0.08 mL of a freshly prepared 2.05 M solution of HI in diethyl ether. The reaction solution was stirred at 25 °C for 12 h. The solution changed color from orange-red to orange. The solution was filtered through neutral alumina in a Schlenk frit. The solvent was removed from the filtrate in vacuo, and the resulting powder was crystallized from CH_2Cl_2/n-hexane (1:3 v/v) at −15 °C. Complex **11** was isolated as orange crystals (46%): mp 189–194 °C; ^1H NMR ($CDCl_3$) δ 1.13 (m, 27, CH_3), 2.05 (m, 6, CH_2), 2.12 (m, 6, CH^A_2), 2.52 (m, 6, CH^B_2), 6.14 (d, 1, CHPh, $^3J_{^{195}Pt-^1H}$ = 58.8 Hz, $^4J_{^{31}P-^1H}$ = 12.6 Hz), 7.10 (m, 3, para Ph, meta Ph), 7.90 (d, 2, ortho Ph, J = 6.92 Hz); $^{31}P\{^1H\}$ NMR (5% $CDCl_3/CHCl_3$) δ 14.3 (s, trans PEt_3, $^1J_{^{195}Pt-^{31}P}$ = 2251 Hz, $^2J_{^{195}Pt-^{31}P}$ = 46.1 Hz), 25.4 (s, PEt_3, $^1J_{^{195}Pt-^{31}P}$ = 5347 Hz, $^2J_{^{195}Pt-^{31}P}$ = 567 Hz). Anal. Calcd for $C_{26}H_{51}P_3Pt_2I_2$: C, 28.37; H, 4.67; P, 8.44. Found: C, 28.46; H, 4.62; P, 7.92.

Preparation of $[Pt_2(\mu\text{-}C{=}CHPh)(PEt_3)_3(NCS)_2]$ (12). To a stirred solution of 0.1 mmol of compound **5** in 10 mL of diethyl ether was added 0.15 mmol of KSCN and 0.05 mL of a 85% solution of HBF_4 in diethyl ether. The reaction solution was stirred at 25 °C for 12 h. The orange solution changed color to pale orange. The solution was filtered through neutral alumina in a Schlenk frit. The solvent was removed from the filtrate in vacuo, and the resulting powder was crystallized from CH_2Cl_2/n-pentane (1:5 v/v) at −15 °C. Complex **12** was isolated as pale orange crystals (76%): mp 160–168 °C; IR (KBr pellet) ν(CN) 2100 (vs) cm^{-1}; ^1H NMR (CD_2Cl_2) major isomer δ 1.23 (m, 27, CH_3), 2.05 (m, 12, CH_2), 2.27 (m, 6, CH_2), 6.20 (d, 1, CHPh, $^4J_{^{31}P-^1H}$ = 11.9 Hz, $^3J_{^{195}Pt-^1H}$ = 46.9 Hz), 7.20, 7.30 (m, 3, para Ph, meta Ph), 8.00 (m, ortho Ph, J = 8.7 Hz); $^{31}P\{^1H\}$ NMR (5% $CDCl_3/CHCl_3$) δ 19.5 (s, trans PEt_3, $J_{^{195}Pt-^{31}P}$ = 2472 Hz, $^2J_{^{195}Pt-^{31}P}$ = 54.7 Hz), 21.0 (s, PEt_3, $^1J_{^{195}Pt-^{31}P}$ = 5217 Hz, $^2J_{^{195}Pt-^{31}P}$ = 617 Hz). Anal. Calcd for $C_{28}H_{51}P_3Pt_2S_2N_2$: C, 34.91; H, 5.34; N, 2.91. Found: C, 34.51; H, 5.56; N, 2.81.

Crystal and Molecular Structural Determinations of Complexes 2 and 10. Crystallographic data are summarized in Table I. Preliminary unit-cell parameters and space group information were derived from oscillation and Weissenberg photographs. Systematic absences established the space group $P2_1/c$ uniquely for **2**. In the case of **10**, two space groups, viz. *Cc* and $C2/c$, were compatible with the systematic absences; solution of the structure showed that the former was correct.

Intensity data ($+h,+k,\pm l$, θ_{max} = 67°; 7393 and 6418 independent measurements for **2** and **10**, respectively) were recorded at 25 °C on an Enraf-Nonius CAD-4 diffractometer [Cu Kα radiation, λ = 1.5418 Å; incident-beam graphite monochromator; ω–2θ scans; scan widths (1.10 + 0.14 tan θ)°, extended 25% on each side for background measurements]. Instrument and crystal

Table I. Crystallographic Data for Complexes 2, 4, and 10

	2	4	10
mol formula	$C_{34}H_{56}ClP_3Pt_2$	$C_{34}H_{56}IP_3Pt_2$	$C_{26}H_{51}Br_2P_3Pt_2$
fw	983.38	1074.76	1006.62
cryst system	monoclinic	orthorhombic	monoclinic
space group	$P2_1/c$ (C_{2h}^5)	$Pbca$ (D_{2h}^{15})	Cc (C_s^4)
a, Å	11.685 (1)	18.004 (3)	10.359 (1)
b, Å	20.810 (7)	22.805 (4)	33.054 (9)
c, Å	19.172 (4)	19.328 (4)	19.855 (5)
β, deg	123.96 (1)	90.0 (...)	93.40 (2)
V, Å^3	3866.8	7935.3	6786.5
Z	4	8	8
D_{calcd}, g cm^{-3}	1.689	1.799	1.970
radiatn, μ, cm^{-1}	Cu Kα, 154.8	Mo Kα, 80.3	Cu Kα, 196.3
cryst dimens, mm	0.13 × 0.13 × 0.35	0.13 × 0.4 × 0.7	0.12 × 0.12 × 0.40
T_{max}:T_{min}	1.00:0.63 (relative)	0.36:0.09 (nonrelative)	1.00:0.67 (relative)
no. of nonequiv reflctns recorded	6907	9126	6063
no. of reflctns retained [$I > 3.0\sigma(I)$]	4517	5341	5585
R (R_w)[a]	0.058 (0.078)	0.045 (0.054)	0.043 (0.058)

[a] $R = \sum||F_o| - |F_c||/\sum|F_o|$; $R_w = [\sum(|F_o| - |F_c|)^2/\sum|F_o|^2]^{1/2}$.

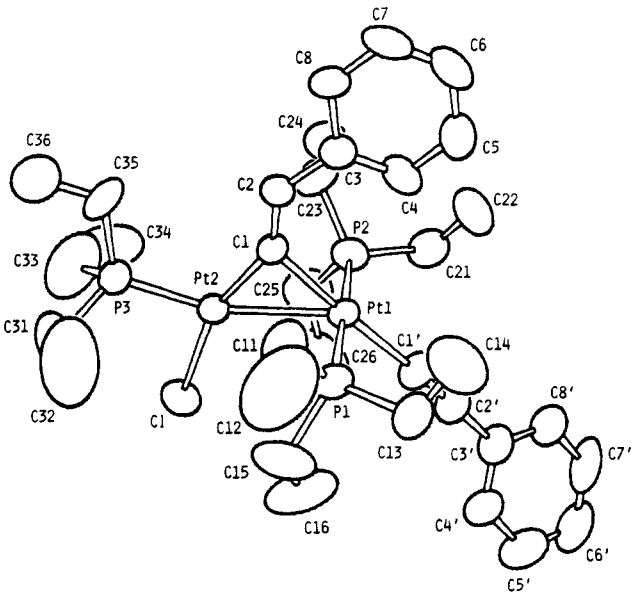

Figure 1. ORTEP diagram (thermal ellipsoids at 33% probability) of complex **2** showing the atomic numbering scheme.

stabilities were monitored throughout by remeasuring the intensities of two control reflections (223, 2$\bar{2}$3 for **2**; 2,10,1, 2,$\bar{10}$,1 for **10**) every 2 h; no significant variation was noted. Refined unit-cell parameters were derived by least-squares treatment of the diffractometer setting angles for 25 reflections ($40° < \theta < 48°$ for **2**; $46° < \theta < 67°$ for **10**) widely separated in reciprocal space. Lorentz–polarization and empirical absorption corrections were applied. Equivalent reflections were then averaged to yield 6909 (**2**) and 6063 (**10**) reflections out of which those 4517 and 5585, respectively, with $I > 3.0\sigma(I)$ were retained for the structure analyses.

Both crystal structures were solved by direct methods.[6] In each case, Pt, P, and Cl/Br atom positions were derived from an E map. Other non-hydrogen atoms were located in a series of difference Fourier syntheses. Hydrogen atoms were included at their calculated positions during the later rounds of full-matrix least-squares refinement of non-hydrogen atom positional and anisotropic temperature factor parameters. A secondary extinction correction, included as a variable in the final least-squares cycles for **10**, refined to 1.8×10^{-7}. Neutral atom scattering factors and their anomalous dispersion corrections were taken from ref 7. In the least-squares iterations, $\sum w\Delta^2$ [$w = 1/\sigma^2(|F_o|)$, $\Delta = (|F_o| - |F_c|)$]

(6) Crystallographic calculations for **2** and **10** were performed on PDP11/44 and Micro VAX II computers by use of the Enraf-Nonius Structure Determination Package incorporating the direct methods program MULTAN11/82.

Table II. Final Atomic Fractional Coordinates (×10^4) for Complex 2 with Estimated Standard Deviations in Parentheses

atom	x	y	z
Pt(1)	3738.2 (4)	1467.3 (2)	1719.1 (3)
Pt(2)	2694.4 (5)	2645.0 (3)	1071.8 (3)
P(1)	4792 (4)	1929 (2)	3037 (2)
P(2)	2585 (3)	1017 (2)	391 (2)
P(3)	2494 (4)	3607 (2)	576 (2)
Cl	543 (3)	2761 (2)	971 (3)
C(1)	4332 (10)	2233 (6)	1303 (7)
C(2)	5438 (10)	2303 (6)	1257 (7)
C(3)	6514 (11)	1841 (7)	1442 (6)
C(4)	6662 (11)	1255 (7)	1781 (9)
C(5)	7680 (16)	837 (8)	1947 (10)
C(6)	8584 (13)	1012 (9)	1710 (10)
C(7)	8484 (12)	1600 (9)	1378 (9)
C(8)	7460 (12)	2002 (7)	1222 (8)
C(1′)	3272 (11)	682 (7)	2156 (8)
C(2′)	2872 (13)	250 (8)	2349 (8)
C(3′)	2357 (12)	−275 (7)	2599 (8)
C(4′)	1718 (14)	−144 (9)	2998 (9)
C(5′)	1171 (16)	−649 (11)	3231 (10)
C(6′)	1320 (15)	−1278 (9)	3072 (12)
C(7′)	1891 (18)	−1401 (8)	2644 (13)
C(8′)	2450 (15)	−915 (9)	2430 (10)
C(11)	6005 (20)	2581 (9)	3253 (10)
C(12)	6752 (36)	2859 (14)	4137 (16)
C(13)	5642 (22)	1410 (9)	3876 (11)
C(14)	6846 (22)	1063 (11)	3985 (15)
C(15)	3524 (20)	2346 (12)	3223 (11)
C(16)	2329 (19)	1942 (17)	2985 (14)
C(21)	2671 (16)	137 (8)	381 (10)
C(22)	4167 (17)	−113 (9)	785 (13)
C(23)	3046 (16)	1328 (8)	−307 (8)
C(24)	2392 (19)	995 (11)	−1152 (10)
C(25)	743 (17)	1189 (12)	−158 (12)
C(26)	102 (16)	1010 (10)	281 (13)
C(31)	2078 (26)	4252 (12)	1042 (14)
C(32)	3104 (38)	4269 (13)	1928 (17)
C(33)	1042 (27)	3775 (14)	−375 (18)
C(34)	302 (24)	3267 (24)	−1014 (16)
C(35)	3924 (18)	3846 (10)	492 (11)
C(36)	3971 (22)	4478 (12)	262 (14)

Table III. Selected Interatomic Distances (Å) and Angles (deg) for Complex 2 with Estimated Standard Deviations

Pt(1)–Pt(2)	2.711 (1)	P(2)–C(21)	1.84 (2)
Pt(1)–P(1)	2.313 (4)	P(2)–C(23)	1.82 (2)
Pt(1)–P(2)	2.312 (3)	P(2)–C(25)	1.83 (2)
Pt(1)–C(1)	2.068 (14)	P(3)–C(31)	1.82 (3)
Pt(1)–C(1′)	2.045 (16)	P(3)–C(33)	1.69 (2)
Pt(2)–P(3)	2.173 (4)	P(3)–C(35)	1.83 (2)
Pt(2)–Cl	2.423 (5)	C(1)–C(2)	1.35 (2)
Pt(2)–C(1)	1.909 (12)	C(2)–C(3)	1.46 (2)
P(1)–C(11)	1.84 (2)	C(1′)–C(2′)	1.17 (2)
P(1)–C(13)	1.72 (2)	C(2′)–C(3′)	1.45 (2)
P(1)–C(15)	1.91 (3)		
Pt(2)–Pt(1)–P(1)	87.3 (1)	Pt(1)–Pt(2)–P(3)	160.9 (1)
Pt(2)–Pt(1)–P(2)	91.5 (1)	Pt(1)–Pt(2)–Cl	107.9 (2)
Pt(2)–Pt(1)–C(1)	44.6 (4)	Pt(1)–Pt(2)–C(1)	49.5 (4)
Pt(2)–Pt(1)–C(1′)	139.1 (3)	Cl–Pt(2)–P(3)	91.1 (2)
P(1)–Pt(1)–P(2)	177.3 (2)	P(3)–Pt(2)–C(1)	111.4 (4)
P(1)–Pt(1)–C(1)	90.7 (4)	Cl–Pt(2)–C(1)	157.5 (4)
P(1)–Pt(1)–C(1′)	89.2 (4)	Pt(1)–C(1)–Pt(2)	85.8 (6)
P(2)–Pt(1)–C(1)	90.2 (4)	Pt(1)–C(1)–C(2)	130.3 (9)
P(2)–Pt(1)–C(1′)	90.1 (4)	Pt(2)–C(1)–C(2)	143.8 (10)
C(1)–Pt(1)–C(1′)	176.2 (5)	Pt(1)–C(1′)–C(2′)	173.3 (10)
C(1)–C(2)–C(3)	129.6 (12)	C(1′)–C(2′)–C(3′)	178.3 (19)

(7) *International Tables for X-Ray Crystallography*; Kynoch Press: Birmingham, England, 1974; Vol. IV.

Table IV. Final Non-Hydrogen Atomic Fractional Coordinates (×10⁴) for Complex 10 with Estimated Standard Deviations in Parentheses

atom	x	y	z
Pt(1)	0 (...)[a]	-269.7 (2)	0 (...)
Pt(2)	1758.8 (7)	288.0 (2)	406.6 (4)
Br(1)	-858 (4)	-969 (1)	70 (2)
Br(2)	3312 (3)	-28 (1)	1280 (1)
P(1)	1437 (5)	-479 (1)	-785 (3)
P(2)	-1305 (5)	-63 (1)	877 (3)
P(3)	2789 (4)	870 (1)	477 (2)
C(1)	289 (16)	325 (5)	-239 (8)
C(2)	-398 (16)	560 (4)	-710 (8)
C(3)	-1459 (19)	462 (6)	-1170 (9)
C(4)	-2130 (22)	98 (7)	-1216 (13)
C(5)	-3223 (25)	19 (10)	-1659 (14)
C(6)	-3661 (25)	329 (9)	-2042 (12)
C(7)	-3113 (26)	697 (8)	-1991 (12)
C(8)	-2040 (24)	751 (8)	-1588 (11)
C(11)	1856 (24)	-89 (7)	-1374 (11)
C(12)	2849 (26)	-216 (9)	-1874 (12)
C(13)	825 (25)	-898 (6)	-1318 (11)
C(14)	-316 (26)	-760 (9)	-1777 (13)
C(15)	2943 (22)	-645 (10)	-374 (16)
C(16)	2752 (29)	-987 (11)	167 (19)
C(21)	-2769 (20)	-353 (6)	933 (14)
C(22)	-3706 (22)	-369 (10)	270 (14)
C(23)	-1806 (19)	466 (8)	841 (11)
C(24)	-2572 (22)	616 (7)	1446 (10)
C(25)	-453 (24)	-126 (8)	1717 (11)
C(26)	47 (33)	-542 (8)	1848 (14)
C(31)	4448 (17)	844 (8)	251 (11)
C(32)	4619 (24)	695 (9)	-462 (14)
C(33)	2897 (22)	1080 (6)	1323 (9)
C(34)	1704 (28)	1129 (10)	1647 (14)
C(35)	2065 (19)	1268 (5)	-56 (9)
C(36)	2765 (26)	1663 (6)	-65 (10)
Pt(1′)	286.1 (7)	2574.1 (2)	-2606.6 (4)
Pt(2′)	-1229.5 (8)	2492.4 (2)	-1562.7 (4)
Br(1′)	594 (3)	3014 (1)	-3603 (1)
Br(2′)	-2845 (3)	3072 (1)	-1576 (2)
P(1′)	-1080 (5)	2167 (1)	-3296 (2)
P(2′)	1550 (5)	3001 (2)	-1928 (3)
P(3′)	-2053 (5)	2238 (2)	-649 (2)
C(1′)	83 (12)	2159 (5)	-1827 (7)
C(2′)	754 (16)	1814 (5)	-1725 (7)
C(3′)	1825 (17)	1650 (5)	-2097 (9)
C(4′)	2627 (25)	1845 (6)	-2517 (13)
C(5′)	3387 (38)	1665 (9)	-2899 (18)
C(6′)	3747 (25)	1262 (8)	-2825 (15)
C(7′)	3025 (22)	1029 (7)	-2393 (14)
C(8′)	2042 (22)	1218 (5)	-2022 (12)
C(11′)	-1883 (30)	1735 (7)	-2935 (14)
C(12′)	-2833 (27)	1490 (8)	-3449 (15)
C(13′)	-9 (51)	1993 (12)	-4072 (16)
C(14′)	809 (64)	1706 (14)	-3898 (38)
C(15′)	-2257 (27)	2437 (8)	-3806 (16)
C(16′)	-3216 (29)	2667 (12)	-3410 (15)
C(21′)	2911 (25)	3212 (7)	-2356 (15)
C(22′)	3831 (27)	2943 (10)	-2620 (17)
C(23′)	2281 (23)	2755 (9)	-1177 (12)
C(24′)	3437 (44)	2990 (16)	-837 (23)
C(25′)	684 (24)	3437 (8)	-1580 (15)
C(26′)	21 (42)	3688 (11)	-2115 (21)
C(31′)	-3781 (26)	2173 (12)	-705 (14)
C(32′)	-4225 (31)	1827 (12)	-1288 (22)
C(33′)	-2050 (32)	2586 (10)	70 (14)
C(34′)	-661 (47)	2704 (14)	244 (18)
C(35′)	-1298 (28)	1775 (6)	-327 (12)
C(36′)	-1855 (33)	1570 (9)	279 (15)

[a] The x and z coordinates of Pt(1) were held constant throughout to define the space group origin in these directions.

was minimized. The maximum shift-to-error in the final least-squares cycle was <0.10, and the standard error of an observation of unit weight was 1.51 for **2** and 1.45 for **10**. The largest peak (2.7 e Å^{-3}) in the final difference Fourier synthesis for **2** was located 1.14 Å from Pt(1) while the corresponding maximum (1.8 e Å^{-3}) for **10** was situated 0.86 Å from Pt(2).

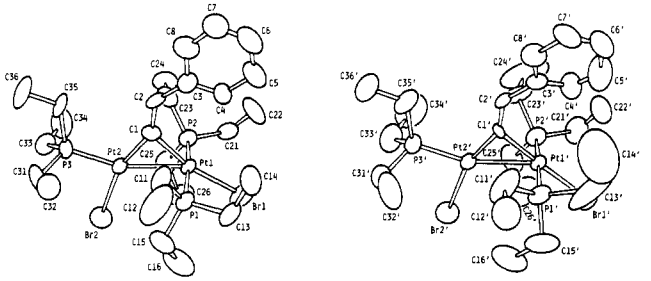

Figure 2. ORTEP plots (thermal ellipsoids at 50% probability) and atom numbering schemes of the two complex molecules in the asymmetric crystal unit of complex **10**. Hydrogen atoms have been omitted for clarity.

Final fractional coordinates for the non-hydrogen atoms of **2** are provided in Table II, and selected distances and angles are listed in Table III. Corresponding parameters and selected distances for **10** are in Tables IV and V. ORTEP diagrams showing the molecular structures and atomic numbering schemes for **2** and **10** are given in Figures 1 and 2, respectively.

Crystal and Molecular Structural Determination of Complex 4. Complex **4** was recrystallized from a THF/hexane (1:5 v/v) solution at -15 °C, and a deep orange, thin octagonal prism was selected. Systematically absent reflections on precession photographs give *Pbca* as the space group. The data crystal was mounted with the long dimension parallel to the ϕ axis of the four-circle diffractometer. Cell constants were determined at 20 °C from a least-squares fit of 2θ, ω, and χ values for 15 reflections ($85° < 2\theta < 89°$) measured at $\pm 2\theta$ with Cu Kα_1 (1.540 56 Å) radiation.

Filtered Mo Kα radiation (0.015 inch Zr foil) was used to measure 9496 reflections (hkl for $10° < 2\theta < 55°$ and $\pm h,\pm k,l$ for $2\theta < 10°$). The Picker FACS-I software[8] measured 2θ step scans and applied a coincidence correction. Nine 0.05° 2θ steps, counted for 2 s each, were centered on the peak, with 10-s backgrounds measured at peak ends. Four reflection standards, measured at intervals, declined 22% in intensity after 200 h of X-ray exposure. The decline was corrected by scaling each interval group. Lorentz–polarization and absorption corrections were made with ORABS[9] using an 8 × 8 × 8 Gaussian grid and μ = 80.28 cm^{-1}. Maximum, minimum, and average transmission factors were 0.36, 0.09, and 0.27. Symmetry-related reflections were averaged to give 9126F_o (including 904 with zero intensity).

The structure was solved by locating the three heavy atoms in a sharpened Patterson function. The remaining atoms were located in a series of difference syntheses. Disorder in the α-carbon atoms of P(2) was approximated by allowing alternate positions (45% occupation, based on the average number of electrons in the peaks as obtained by integration). Refinement was by full-matrix least squares with anisotropic thermal parameters. The quantity minimized was $\sum w(|F_o| - |F_c|)^2$ where $w = 1/\sigma^2(F_o)$ and the variance, σ^2, was based on counting statistics and included the usual instability term (4%). Atomic scattering factors were from Cromer and Mann,[10] and anomalous-dispersion factors (all atoms) were those of Cromer and Liberman.[11] The maximum shift-to-error for the final refinement cycle was 0.25. Maximum and minimum $\Delta\rho$ values were 1.8 and -1.2 e Å^{-3}, near Pt(2) and I, respectively. The standard error of an observation of unit weight was 1.6. Least-squares refinement, structure factors, electron density, least-squares planes, bond distances, and bond angles were calculated with the X-ray 67 programs as implemented and updated on the Vanderbilt DEC-1099 computer.[12]

(8) Lenhert, P. G. *J. Appl. Crystallogr.* **1975**, *8*, 569–570.
(9) Wehe, D. J.; Busing, W. R.; Levy, H. A. ORABS, *A Fortran Program for Calculating Single Crystal Absorption Corrections*, Report ORNL-TM-229, 1962; Oak Ridge National Laboratory, Oak Ridge, TN.
(10) Cromer, D. T.; Mann, J. B. *Acta Crystallogr., Sect. A* **1968**, *A24*, 321–324.
(11) Cromer, D. T.; Liberman, D. *J. Chem. Phys.* **1970**, *53*, 1891–1898.
(12) Stewart, J. M. *X-ray 67 Program System for X-ray Crystallography*, Technical Report TR-67-58, 1967; Computer Science Center, University of Maryland, College Park, MD.

Table V. Selected Interatomic Distances (Å) and Angles (deg) for Complex 10 with Estimated Standard Deviations

	unprimed molecule	primed molecule		unprimed molecule	primed molecule
Pt(1)–Pt(2)	2.682 (1)	2.687 (1)	C(1)–C(2)	1.38 (2)	1.34 (2)
Pt(1)–Br(1)	2.483 (3)	2.491 (3)	C(2)–C(3)	1.42 (2)	1.47 (2)
Pt(1)–P(1)	2.324 (6)	2.336 (4)	C(3)–C(4)	1.39 (3)	1.37 (3)
Pt(1)–P(2)	2.368 (6)	2.305 (6)	C(3)–C(8)	1.38 (3)	1.45 (2)
Pt(1)–C(1)	2.05 (2)	2.09 (2)	C(4)–C(5)	1.42 (3)	1.27 (4)
Pt(2)–Br(2)	2.521 (3)	2.543 (3)	C(5)–C(6)	1.34 (4)	1.39 (4)
Pt(2)–P(3)	2.200 (4)	2.216 (5)	C(6)–C(7)	1.34 (4)	1.40 (4)
Pt(2)–C(1)	1.94 (2)	1.85 (1)	C(7)–C(8)	1.34 (3)	1.43 (3)
P(1)–C(11)	1.81 (2)	1.82 (3)	C(11)–C(12)	1.53 (4)	1.60 (4)
P(1)–C(13)	1.83 (2)	2.03 (4)	C(13)–C(14)	1.52 (4)	1.30 (7)
P(1)–C(15)	1.80 (3)	1.78 (3)	C(15)–C(16)	1.58 (5)	1.51 (4)
P(2)–C(21)	1.80 (2)	1.83 (3)	C(21)–C(22)	1.59 (4)	1.43 (4)
P(2)–C(23)	1.82 (3)	1.82 (3)	C(23)–C(24)	1.56 (3)	1.55 (5)
P(2)–C(25)	1.85 (2)	1.85 (3)	C(25)–C(26)	1.49 (4)	1.48 (5)
P(3)–C(31)	1.80 (2)	1.80 (3)	C(31)–C(32)	1.52 (4)	1.67 (5)
P(3)–C(33)	1.81 (2)	1.83 (3)	C(33)–C(34)	1.44 (4)	1.51 (6)
P(3)–C(35)	1.82 (2)	1.82 (2)	C(35)–C(36)	1.49 (3)	1.52 (4)
Pt(2)–Pt(1)–Br(1)	149.5 (1)	141.2 (1)	P(1)–Pt(1)–C(1)	91.3 (5)	88.4 (4)
Pt(2)–Pt(1)–P(1)	87.5 (1)	91.9 (1)	P(2)–Pt(1)–C(1)	89.5 (5)	92.7 (4)
Pt(2)–Pt(1)–P(2)	89.3 (1)	87.0 (1)	Pt(1)–Pt(2)–Br(2)	108.5 (1)	109.3 (1)
Pt(2)–Pt(1)–C(1)	45.9 (4)	43.4 (4)	Pt(1)–Pt(2)–P(3)	159.7 (1)	160.2 (2)
Br(1)–Pt(1)–P(1)	90.3 (1)	88.4 (1)	Pt(1)–Pt(2)–C(1)	49.5 (5)	50.8 (5)
Br(1)–Pt(1)–P(2)	90.3 (1)	90.7 (2)	Br(2)–Pt(2)–P(3)	91.8 (1)	90.5 (2)
Br(1)–Pt(1)–C(1)	164.6 (5)	174.5 (4)	Br(2)–Pt(2)–C(1)	157.9 (5)	160.1 (5)
P(1)–Pt(1)–P(2)	174.7 (2)	177.0 (2)	P(3)–Pt(2)–C(1)	110.3 (5)	109.3 (5)
Pt(1)–P(1)–C(11)	114.1 (8)	119.7 (9)	Pt(2)–C(1)–C(2)	147 (1)	148 (1)
Pt(1)–P(1)–C(13)	113.5 (8)	105.6 (13)	C(1)–C(2)–C(3)	131 (1)	129 (1)
Pt(1)–P(1)–C(15)	111.0 (10)	114.6 (9)	C(2)–C(3)–C(4)	127 (2)	129 (2)
C(11)–P(1)–C(13)	104.7 (10)	111.0 (15)	C(2)–C(3)–C(8)	121 (2)	115 (2)
C(11)–P(1)–C(15)	106.0 (13)	107.7 (13)	C(4)–C(3)–C(8)	111 (2)	115 (2)
C(13)–P(1)–C(15)	107.0 (13)	95.6 (16)	C(3)–C(4)–C(5)	125 (2)	124 (2)
Pt(1)–P(2)–C(21)	114.3 (8)	112.9 (9)	C(4)–C(5)–C(6)	116 (3)	124 (3)
Pt(1)–P(2)–C(23)	114.9 (7)	113.5 (9)	C(5)–C(6)–C(7)	122 (2)	116 (3)
Pt(1)–P(2)–C(25)	111.6 (8)	115.1 (8)	C(6)–C(7)–C(8)	120 (2)	120 (2)
C(21)–P(2)–C(23)	105.9 (9)	104.8 (12)	C(3)–C(8)–C(7)	126 (2)	119 (2)
C(21)–P(2)–C(25)	104.0 (12)	106.3 (12)	P(1)–C(11)–C(12)	115 (2)	115 (2)
C(23)–P(2)–C(25)	105.2 (11)	103.2 (13)	P(1)–C(13)–C(14)	110 (2)	112 (4)
Pt(2)–P(3)–C(31)	114.1 (9)	115.1 (10)	P(1)–C(15)–C(16)	113 (2)	114 (2)
Pt(2)–P(3)–C(33)	113.3 (7)	114.6 (10)	P(2)–C(21)–C(22)	116 (2)	119 (2)
Pt(2)–P(3)–C(35)	114.4 (6)	115.4 (9)	P(2)–C(23)–C(24)	116 (2)	114 (2)
C(31)–P(3)–C(33)	104.0 (10)	94.5 (15)	P(2)–C(25)–C(26)	114 (2)	112 (2)
C(31)–P(3)–C(35)	104.8 (10)	109.1 (15)	P(3)–C(31)–C(32)	114 (1)	111 (2)
C(33)–P(3)–C(35)	105.2 (9)	105.9 (12)	P(3)–C(33)–C(34)	117 (2)	107 (2)
Pt(1)–C(1)–Pt(1)	84.6 (6)	85.8 (6)	P(3)–C(35)–C(36)	117 (1)	118 (2)
Pt(1)–C(1)–C(2)	128 (1)	127 (1)			

Relevant crystallographic data for complex **4** are provided in Table I. Values of the final atomic fractional coordinates for compound **4** are shown in Table VI, and selected interatomic distances and angles are listed in Table VII. An ORTEP[13] diagram showing the molecular structure and the atomic numbering scheme for complex **4** is provided in Figure 3.

Photophysical Studies of Complexes 1a and 2. Room-temperature absorption spectra of complexes **1a** and **2** were recorded by using a Hewlett-Packard 8452A diode-array spectrophotometer. Measurements were made for each complex in both CH_2Cl_2 and ethanol.

Emission and excitation spectra were recorded on a Spex Fluorolog 2 spectrofluorimeter. Emission spectra were corrected for solvent background and instrumental response, and excitation spectra were background corrected only. Room-temperature measurements were made in deaerated CH_2Cl_2 solutions while low temperature (77 K) measurements employed 4:1 ethanol/methanol glasses.

Attempts to measure the emission spectra of **1a** were made at 298 K and 77 K by using excitation into the 290 and 400 nm absorption maxima. Spectra of complex **2** used 410 and 488 nm excitation. A low-temperature excitation spectrum was run of complex **2** monitoring the emission at its corrected maximum (696 nm).

Absolute luminescence quantum yields (Φ) of complex **2** were measured at 77 K by the Parker–Rees method[14,15] using $[Ru(bpy)_3]Cl_2$ [$\Phi = 0.376$][16] as a standard. Measurements of both the standard and **2** in 4:1 ethanol/methanol glasses used 410-nm excitation. In the absence of low-temperature absorption spectra,

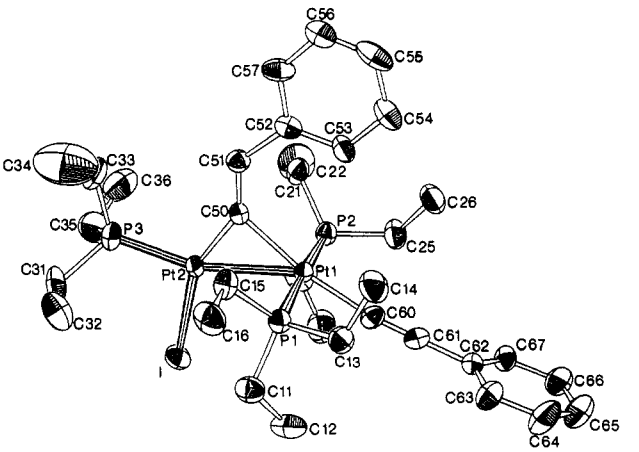

Figure 3. ORTEP diagram (thermal ellipsoids at 30% probability) of complex **4** showing the atomic numbering scheme.

(13) Johnson, C. K. ORTEP-II, Report ORNL-5138, 1976; Oak Ridge National Laboratory, Oak Ridge, TN.

(14) Parker, C. A.; Rees, W. T. *Analyst (London)* **1962**, *87*, 83–111.
(15) Demas, J. N.; Crosby, G. A. *J. Phys. Chem.* **1971**, *75*, 991–1024.
(16) Demas, J. N.; Crosby, G. A. *J. Am. Chem. Soc.* **1971**, *93*, 2841–2847.

Table VI. Final Fractional Coordinates for Complex 4 with Estimated Standard Deviations in Parentheses

atom	x	y	z
Pt(1)	2229.2 (2)	1174.2 (2)	1528.1 (2)
Pt(2)	2912.0 (2)	113.4 (2)	1631.5 (2)
I	1826.3 (5)	-629.3 (4)	2019.0 (5)
P(1)	1940 (2)	939 (1)	396 (1)
P(2)	2418 (2)	1377 (1)	2687 (1)
P(3)	3781 (2)	-561 (2)	1593 (2)
C(11)	1286 (7)	342 (5)	330 (5)
C(12)	545 (7)	443 (6)	731 (6)
C(13)	1471 (6)	1523 (5)	-85 (5)
C(14)	1921 (8)	2071 (6)	-143 (7)
C(15)	2735 (6)	731 (5)	-136 (6)
C(16)	2543 (7)	611 (5)	-924 (6)
C(21)[a]	3353 (14)	1347 (12)	2997 (13)
C(22)	3401 (12)	1238 (8)	3799 (9)
C(23)[a]	1963 (16)	773 (11)	3209 (10)
C(24)	1177 (9)	763 (8)	3147 (10)
C(25)[a]	1948 (14)	2026 (10)	3011 (12)
C(26)	2228 (8)	2624 (6)	2636 (8)
C(41)[b]	3271 (25)	939 (14)	3101 (15)
C(43)[b]	1629 (15)	1403 (16)	3242 (12)
C(45)[b]	2724 (20)	2195 (14)	2809 (14)
C(31)	3552 (9)	-1248 (5)	1167 (8)
C(32)	3293 (12)	-1164 (8)	469 (10)
C(33)	4654 (10)	-343 (10)	1338 (17)
C(34)	4951 (17)	-428 (14)	767 (13)
C(35)	3927 (10)	-914 (7)	2437 (10)
C(36)	4281 (9)	-548 (8)	2922 (10)
C(50)	3319 (5)	860 (4)	1416 (4)
C(51)	3962 (5)	1137 (5)	1276 (5)
C(52)	4083 (6)	1792 (5)	1156 (5)
C(53)	3515 (7)	2208 (5)	1169 (5)
C(54)	3674 (8)	2801 (5)	1047 (6)
C(55)	4423 (9)	2945 (6)	955 (6)
C(56)	4973 (7)	2548 (6)	948 (6)
C(57)	4801 (6)	1979 (5)	1052 (5)
C(60)	1269 (5)	1624 (5)	1569 (4)
C(61)	763 (5)	1946 (5)	1563 (5)
C(62)	135 (6)	2362 (4)	1541 (5)
C(63)	-114 (6)	2624 (5)	2145 (5)
C(64)	-695 (7)	3037 (6)	2092 (6)
C(65)	-1031 (8)	3151 (7)	1472 (7)
C(66)	-764 (8)	2874 (7)	879 (7)
C(67)	-204 (7)	2462 (6)	892 (6)

[a] Occupancy factor = 0.55. [b] Occupancy factor = 0.45.

Table VII. Selected Interatomic Distances (Å) and Angles (deg) for Complex 4 with Estimated Standard Deviations

Pt(1)-Pt(2)	2.721 (1)	P(2)-C(25)	1.82 (2)
Pt(1)-P(1)	2.313 (3)	P(2)-C(41)	2.00 (4)
Pt(1)-P(2)	2.312 (3)	P(2)-C(43)	1.78 (3)
Pt(1)-C(50)	2.099 (9)	P(2)-C(45)	1.96 (3)
Pt(1)-C(60)	2.012 (10)	P(3)-C(31)	1.818 (14)
Pt(2)-P(3)	2.195 (3)	P(3)-C(33)	1.72 (2)
Pt(2)-I	2.693 (1)	P(3)-C(35)	1.84 (2)
P(1)-C(11)	1.804 (12)	C(50)-C(51)	1.347 (13)
P(1)-C(13)	1.829 (11)	C(51)-C(52)	1.528 (14)
P(1)-C(15)	1.825 (11)	C(60)-C(61)	1.171 (14)
P(2)-C(21)	1.79 (3)	C(61)-C(62)	1.475 (14)
P(2)-C(23)	1.89 (3)	Pt(2)-C(50)	1.900 (9)
Pt(2)-Pt(1)-P(1)	88.00 (7)	Pt(1)-Pt(2)-P(3)	160.49 (9)
Pt(2)-Pt(1)-P(2)	92.29 (7)	Pt(1)-Pt(2)-I	104.58 (2)
Pt(2)-Pt(1)-C(50)	44.1 (3)	Pt(1)-Pt(2)-C(50)	50.3 (3)
Pt(2)-Pt(1)-C(60)	147.0 (3)	I-Pt(2)-P(3)	94.91 (9)
P(1)-Pt(1)-P(2)	174.98 (10)	P(3)-Pt(2)-C(50)	110.3 (3)
P(1)-Pt(1)-C(50)	91.9 (2)	I-Pt(2)-C(50)	154.8 (3)
P(1)-Pt(1)-C(60)	87.8 (3)	Pt(1)-C(50)-Pt(2)	85.6 (4)
P(2)-Pt(1)-C(50)	91.8 (2)	Pt(1)-C(50)-C(51)	131.7 (7)
P(2)-Pt(1)-C(60)	89.3 (3)	Pt(2)-C(50)-C(51)	142.7 (8)
C(50)-Pt(1)-C(60)	168.8 (4)	Pt(1)-C(60)-C(61)	171.3 (10)
C(50)-C(51)-C(52)	127.7 (9)	C(60)-C(61)-C(62)	178.4 (10)

we assume that the ratios of the sample to reference absorbance at room temperature were maintained at 77 K. The yield of **2** is the average of three sets of four measurements with the sample being removed and replaced in the sample holder between each set.

Excited state lifetimes (τ) were measured by using a pulsed N_2 laser (337-nm) nanosecond decay system and software described elsewhere.[17] The same optical Dewar used for emission spectra was used in the lifetime measurements. The nonexponential decays were fit by nonlinear least squares[18] to the sum of two exponentials (eq 1) where $I(t)$ is the luminescence intensity

$$I(t) = K_s \exp(-t/\tau_s) + K_l \exp(-t/\tau_l) \quad (1)$$

at a time t and the K's and τ's are the preexponential weighting factors and the excited-state lifetimes, respectively. The subscripts s and l refer to the short- and long-lived components, respectively.

Radiative, k_r, and nonradiative, k_{nr}, decay constants and the radiative or intrinsic lifetime, τ_r, were calculated from

$$k_r = \Phi/\tau \quad (2a)$$

$$k_{nr} = (1 - \Phi)/\tau \quad (2b)$$

$$\tau_r = 1/k_r \quad (2c)$$

where Φ is the absolute quantum yield and τ is the observed lifetime under the same conditions. τ_r is the lifetime that would be observed if there were no radiationless deactivation of the excited state. These expressions assume that the intersystem crossing efficiency is unity. For a series of platinum metal complexes (Ru(II) and Os(II) with α-diimine ligands), this has been shown to be true.[16] Further, it is clear that the intersystem crossing yield for $Pt_2(POP)_4^{4-}$ is very high since the fluorescence is a minor contribution to the total emission. Therefore, in the current systems, a unit intersystem crossing yield is a reasonable assumption. Furthermore, in the current systems, calculations were carried out by taking an average of the two components of the nonexponential decay.

Results

Complex **1** has been treated separately with 35 inorganic, organic, or organometallic nucleophiles with the anticipation of forming neutral, diplatinum complexes including products that would have increased nuclearity or hydrocarbyl ligand content. Within these expectations, complex **1** formed neutral, diplatinum complexes only upon reaction with halide, pseudohalide, or RS^- nucleophiles, as shown in eq 3. The propensity of **1** to react only with ligands

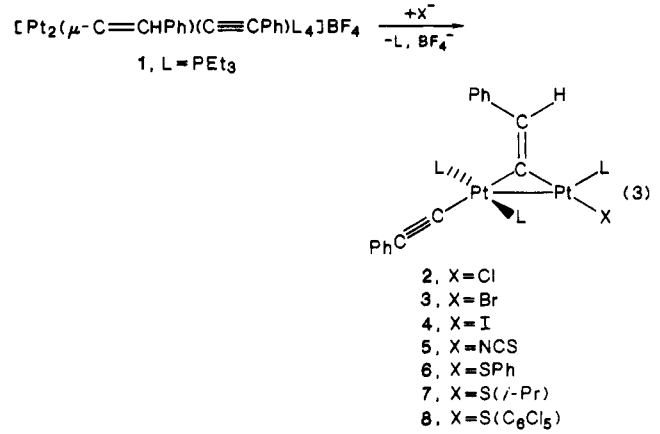

2, X = Cl
3, X = Br
4, X = I
5, X = NCS
6, X = SPh
7, X = S(*i*-Pr)
8, X = S(C_6Cl_5)

having electronegative donor atoms is substantiated further by the observation that while complex **1** does not react with halide-free methyllithium, it does react with MeLi·LiBr to give the Pt_2Br compound **3**. One PEt_3 ligand of **1** is lost during the formation of products **2**–**8**. These

(17) (a) Turley, T. J. M.S. Thesis, University of Virginia, 1980. (b) Turley, T. J.; Demas, J. N. *Anal. Chim. Acta* **1987**, *197*, 121–128.
(18) (a) Daniels, R. W. *An Introduction to Numerical Methods and Optimization Techniques*; North-Holland: New York, 1978. (b) Demas, J. M. *Excited State Lifetime Measurements*; Academic: New York, 1983.

neutral, diplatinum compounds are isolated in yields ranging from 54 to 75%.

Both structural and NMR[2,3] data confirm unambiguously the molecular structure shown for compounds **2–8**. Each product contains a μ-phenylethenylidene ligand having the same isomer structure as that observed for compound **1a**. Both isomers of **1** (**1a** or **1b**) react with these nucleophiles to give products **2–8**. However, qualitative observations indicate that isomer **1b** forms the product complexes at a rate approximately four times slower than the rate of reaction of isomer **1a** with the same nucleophile. Presumably, the μ-phenylethenylidene ligand of **1b** must undergo isomerization to the structure shown for **1a** before reaction with a nucleophile can be completed.

The X-ray structures of the Pt_2Cl complex **2** and the Pt_2I complex **4** have been determined. Relevant crystallographic and structural data for compound **2** are shown in Tables I–III, and similar data for complex **4** are shown in Tables I, VI, and VII. ORTEP diagrams showing the molecular structures and atomic numbering schemes for **2** and **4** are provided in Figures 1 and 3, respectively.

Complexes **2** and **4** have very similar structures with Pt(1)–Pt(2) distances of 2.711 (1) and 2.721 (1) Å, respectively. The coordination geometry about Pt(1) is nearly square-planar [excluding Pt(2)] with P(1) and P(2) occupying trans coordination sites. The coordination geometry about Pt(2) reveals a distorted "Y-shaped" structure. The Pt(2)–Cl and Pt(2)–I distances of 2.423 (5) and 2.693 (1) Å, respectively, indicate that Pt(2) has a single-bond covalent radius of ca. 1.40 Å. A phenylethenylidene ligand bridges Pt(1) and Pt(2) in both molecules. The alkenylidene donor atom is positioned nearly trans to the terminal phenylacetylide ligand on Pt(1), and it forms a shorter bond to Pt(2) than it does to Pt(1) by ca. 0.18 Å. The C=C double bond distance within each phenylethenylidene ligand is 1.35 (2) Å. The stereochemistry about this bond places the phenyl group trans to Pt(2). The C≡C triple bond distance within the phenylacetylide ligands of **2** and **4** is 1.17 (2) Å. Overall, both molecules have idealized mirror symmetry where a plane of symmetry containing the atoms [Pt(1), Pt(2), P(3), Cl, C(1), C(2) and C(1′) as in complex **2**, for example] is evident, thereby making the P(1) and P(2) PEt_3 ligands symmetry equivalent. In complex **2**, for example, the maximum atomic deviation from this plane is −0.041 Å for P(3), and the atoms C(3), C(4), C(2′) and C(3′) are displaced 0.13, 0.11, 0.04, and 0.08 Å, respectively, from this plane.

A FAB–mass spectrum of the Pt_2Br compound **3** reveals a $(\text{parent} - Br)^+$ peak at m/e 948. Infrared spectra of **2–4** and **6–8** show a weak band between 2110 and 2115 cm^{-1} for the C≡C stretching vibration of the phenylacetylide ligand. Complex **5** exists as two linkage isomers of ca. 2:1 relative abundance. The major isomer has a ν_{CN} band at 2085 cm^{-1} and is assigned to the isothiocyanate isomer.[19] Because of peak overlap, the C–S stretching band is not evident in the IR spectrum of this compound. This isomer assignment is supported by ^1H NMR data (vide infra) in that the resonance for the alkenylidene proton of the minor isomer appears at a chemical shift value similar to that observed for the Pt_2SR compounds (which also contain sulfur donor atoms).

The ^1H NMR data of complexes **2–8** can be readily interpreted on the basis of a previous analysis of the NMR spectrum of complex **1**.[3] For complex **1a**, the alkenylidene proton resonance appears as a doublet of doublets at δ 7.73 ppm [due to $^4J_{PH}$ coupling of 21.5 and 9.9 Hz to the two PEt_3 ligands coordinated to Pt(2)] and the resonance of the ortho protons of the phenyl substituent of the phenylethenylidene ligand appears as a distinct doublet at δ 7.92 ppm. For complexes **2–5** and **8**, the alkenylidene proton resonance is observed as a doublet [due to $^4J_{PH}$ coupling of ca. 18 Hz to the single PEt_3 ligand coordinated to Pt(2)] in the range δ 6.75–6.95 ppm, and the doublet resonances for the ortho protons of the phenylethenylidene ligands in **2–8** appear in the range δ 7.75–7.90 ppm. Furthermore, the low symmetry of compounds **2–8** makes the methylene protons within each of the P(1) and P(2) PEt_3 ligands diastereotopic, and, therefore, anisochronous. In complex **3**, this anisochronism is ca. 0.45 ppm.

The ^{31}P-NMR spectra of compounds **2–6** and **8** have been recorded and can be analyzed by first-order methods as an 18-line pattern arising from a superposition of the properly weighted resonances for the four isotopomers expected in such diplatinum molecules. The ^{31}P NMR spectra of compounds **3**, **4**, and **6** show all 18 lines; however, the presence of isomers, low resolution, or possibly second-order effects obscure as many as four of the expected resonances for the most minor isotopomer (11.4% relative abundance) in the spectra of the remaining complexes. The resonance for the two equivalent PEt_3 ligands appears in the range δ 11.6–15.6 ppm with $^1J_{Pt-P}$ and $^2J_{Pt-P}$ coupling constants in the ranges of 2194–2244 and 34.9–52.8 Hz, respectively. $^3J_{PP}$ coupling is not observed. While the values for $^1J_{Pt-P}$ coupling are typical,[20] the values of $^2J_{Pt-P}$ are lower than usual due, presumably, to the nearly perpendicular alignment of the P(1)–P(2) vector relative to the Pt(1)–Pt(2) vector. The ^{31}P resonance for the unique PEt_3 ligand occurs in the range δ 23.0–31.3 ppm with $^1J_{Pt-P}$ and $^2J_{Pt-P}$ coupling constants in the ranges of 5372–5672 and 376–419 Hz, respectively. These unusually large coupling constants might indicate some degree of Pt → Pt mixed-valence character in these compounds in analogy to the NMR analysis of the Pt–P coupling observed in $Pt_2Br_2(\mu\text{-CO})(PPh_3)_3$ and related complexes as reported by Goodfellow et al.[21]

Further reactivity studies with complex **1** indicate that it does not react with strong Brønsted bases of low nucleophilicity to effect deprotonation of the phenylethenylidene ligand, nor does it react with various carbene or M–M bond insertion reagents.[22] However, complex **1** does react with protic acids, HX, to eliminate the terminal phenylacetylide ligand as phenylacetylene (determined by TLC). This Pt–C cleavage reaction can be used to prepare Pt_2X_2 derivatives, as shown in eq 4. Complex **10** (Pt_2Br_2) can also be prepared by treating **1a** with either HBF_4 or HPF_6 followed by the addition of LiBr (respective yields are 63 and 70%).

Compounds **9–12** are isolated in yields of 46–76%. The X-ray structure of the Pt_2Br_2 complex **10** has been determined. Relevant crystallographic and structural data

(19) Burmeister, J. L.; Basolo, F. *Inorg. Chem.* **1964**, *3*, 1587–1593.

(20) (a) Pregosin, P. S. In *Methods of Stereochemical Analysis*; Verkade, J. G., Quin, L. D., Eds.; VCH Publishers, Inc.: Deerfield Beach, FL, 1987; Vol. 8, pp 465–530. (b) Crumbliss, A. L.; Topping, R. J. ref 20a, pp 531–557. (c) Nixon, J. F.; Pidcock, A. ^{31}P NMR Spectra of Co-ordinated Compounds. In *NMR Spectroscopy*; Mooney, E. F., Ed.; Academic: New York, 1969; Vol. 2, pp 345–422. (d) Pregosin, P. S.; Kunz, R. W. ^{31}P and ^{13}C NMR of Transition Metal Phosphine Complexes. *NMR Basic Principles and Progress*; Diehl, P., Fluck, E., Kosfield, R., Eds.; Springer-Verlog: New York, 1979; Vol. 16.

(21) Goodfellow, R. J.; Herbert, I. R.; Orpen, A. G. *J. Chem. Soc., Chem. Commun.* **1983**, 1386–1388.

(22) (a) Casey, C. P.; Marder, S. R. *Organometallics* **1985**, *4*, 411–413. (b) Hoel, E. L.; Ansell, G. B.; Leta, S. *Organometallics* **1984**, *3*, 1633–1637. (c) Jacobsen, E. N.; Bergman, R. G. *Organometallics* **1984**, *3*, 329–331. (d) Brum, P.; Dawkins, G. M.; Green, M.; Mills, R. M.; Salaun, J.-Y.; Stone, F. G. A.; Woodward, P. *J. Chem. Soc., Chem. Commun.* **1981**, 966–968.

$$[Pt_2(\mu\text{-}C{=}CHPh)(C{\equiv}CPh)L_3X] \xrightarrow[-PhC\equiv CH]{+H^+,\ X^-}$$

2, X = Cl
3, X = Br
4, X = I
5, X = NCS

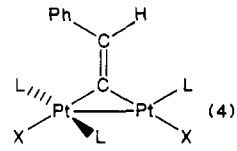

(4)

9, X = Cl
10, X = Br
11, X = I
12, X = NCS

are provided in Tables I, IV, and V, and an ORTEP diagram showing the molecular structure of **10** and the atomic numbering scheme is provided in Figure 2.

Compound **10** crystallizes as two independent molecules per asymmetric unit. The molecular structure of **10** is related to that of **2** and **4** in that the halogen bonded to Pt(2) is now Br and that the terminal phenylacetylide ligand attached to Pt(1) is now replaced by a Br ligand. The Pt(1)–Pt(2) distances for the two molecules are 2.682 (1) and 2.687 (1) Å. The average values for the Pt(2)–Br(2) and Pt(1)–Br(1) distances are, respectively, ca. 2.53 and 2.48 Å. The stereochemistry of the coordination geometries about Pt(1) and Pt(2) and about the C=C double bond of the bridging phenylethenylidene ligand in **10** is directly analogous to that found in compounds **2** and **4**. The values of the C(1)=C(2) double bond distances are 1.38 (2) and 1.34 (2) Å. Overall, complex **10** also has idealized C_s symmetry.

Complexes **9–12**, like **2–8**, can exhibit isomerization of the μ-phenylethenylidene ligand like that shown for **1a** and **1b**, although in some cases one isomer can be isolated as a pure material with considerable effort. The ^1H NMR spectra of **9–12** show the expected doublet resonance for the alkenylidene proton in the range δ 6.10–6.20 ppm. This resonance appears at ca. 0.70 ppm to higher field than does the corresponding resonance for the Pt_2X compounds. The value of the $^4J_{PH}$ coupling constant is ca. 12 Hz, and platinum satellites on these resonances are observed due to $^3J_{PtH}$ coupling of ca. 43–59 Hz. A doublet resonance due to the ortho protons of the bridging phenylethenylidene ligand appears in the range δ 7.89–8.00 ppm, as expected. The anisochronism observed between the resonances of the methylene protons within the two equivalent PEt_3 ligands ranges from ca. 0.30 to 0.40 ppm. Complex **12** has a ν(CN) stretching band at 2100 cm^{-1} in the IR spectrum; however, the ^1H NMR spectrum of **12** indicates that four possible isomers are present (presumably due to linkage isomerism). Two of these isomers are present in a greater relative abundance compared to that of the other two isomers.

The ^{31}P NMR spectra of compounds **9–12** can also be analyzed as first-order spectra. The ^{31}P spectrum of the Pt_2I_2 compound **11** shows the complete 18-line spectrum as expected under a first-order analysis. The spectra of the other compounds lack up to four of the resonances expected for the minor isotopomer. The ^{31}P resonance of the two equivalent PEt_3 ligands appears in the range δ 13.8–19.5 ppm with $^1J_{Pt-P}$ and $^2J_{Pt-P}$ coupling constants in the ranges of 2251–2472 and 47.0–54.7 Hz, respectively. These values are very similar to those recorded for the two equivalent PEt_3 nuclei in the Pt_2X compounds. The ^{31}P resonance of the unique PEt_3 ligand appears in the range δ 20.7–25.4 ppm with $^1J_{Pt-P}$ and $^2J_{Pt-P}$ values in the ranges of 5217–5481 and 567–617 Hz, respectively. The values for $^2J_{Pt-P}$ coupling observed in the Pt_2X_2 compounds are significantly larger than those observed for the Pt_2X complexes. This result might by explained by the shorter Pt–Pt distances within the Pt_2X_2 compounds.

Preliminary SC-MEH-MO calculations[23] have been carried out on complex **1a** utilizing the X-ray structural data reported earlier for this cationic complex.[2] The atomic numbering scheme used in the theoretical calculations is the numbering scheme reported with the structural data, and this scheme is identical with that shown in Figure 3 for complex **4** except that the iodine atom must be replaced by a PEt_3 ligand labeled as P(4).

The LCAO format was constructed from quasi-relativistic wave functions for the 5s, 5p, 5d, 6s, and 6p orbitals of the Pt atoms and non relativistic functions of the 3s and 3p orbitals of P, the 2s and 2p orbitals of C, and the 1s orbital of H. Specific details of the computational procedure are the same as those reported earlier.[23]

Because of limitations imposed by the large number of atoms and their respective orbitals pertinent to a complete bonding description of the complex, the following approximations were necessarily invoked. Ethyl groups attached to the P atom ligands are modeled as single C atoms (labeled $Et_{"eff"}$) each having seven valence electrons, with a two orbital composition (a s and a p type) that is 18% C 2s, 53% C 2p, and 29% H 1s in character. In a like manner, each of the protonated five C atoms in the phenyl rings (Ph) is modeled as a single C atom (labeled $CH_{"eff"}$) having five valence electrons, with a two orbital composition that is 27% C 2s, 53% C 2p, and 20% H 1s character. The sixth ligating C atom in the Ph ring is assigned four valence electrons, with a two orbital composition having 33% 2s and 67% 2p character. Therefore, the computationally manageable composition of the entire complex ion contains the following atomic components: Pt atoms, 2; P atoms, 4; $C(Et_{"eff"})$, 12; C(in C=C), 2; C(in C≡C), 2, $C(CH_{"eff"})$, 10, C(ligating C in Ph), 2, H(in C=C—H), 1. This totals 35 atomic components rather than 117 atoms comprising the full, unrestricted molecular unit. The computer program used in these calculations is limited to 50 atoms and 100 orbital types. This modeled system is a 35-atom, 75-orbital problem, which generates 155 total molecular orbitals (MO) to accommodate 214 electrons.

Because of the very low molecular symmetry, no attempt is made to assign symmetry labels to the MO. Furthermore, there is no clear distinction between σ and π bonding in the Pt bonding region of this complex. Those MO numbered 38 through 155 are of negative energy, and MO 49 through 155 are all doubly occupied. MO 38 thru 48 are unoccupied, as are MO 1 through 37, but the latter are above zero in energy. More specific details of the results are presented in Tables VIII–XI, but these initial data have not yet been refined for spin pairing and ligand field effects, which are essential for an adequate rationalization of electronic spectral and magnetic properties. Table VIII includes relative orbital energies and percent atomic orbital (AO) character of the HOMO and LUMO and some general energy ranges of the other MO. Note that the HOMO contains only 3.6% Pt character and is composed primarily of vinylidene Ph and bridging vinylidene C_{50} atom character. The LUMO is only 0.36 eV above the HOMO and is essentially acetylene Ph character, with only 4.1% Pt character. The Pt character increases in the deeper levels and is maximized in MO 82, 84, and 93, with total Pt contributions of approximately 29, 34 and 31%, respec-

(23) Boudreaux, E. A.; Doussa, S. P.; Klobukowski, M. *Int. J. Quantum Chem.: Quantum Chem. Symp.* **1986**, *20*, 239–252 and ref 14, 15, 16, and 17 cited in this publication.

Table VIII. Some Molecular Orbital Energies and HOMO/LUMO Percent AO Contributions of 1a[a]

MO (no.)	E, eV	Pt_1 5d	Pt_1 6s	Pt_1 6p	Pt_2 5d	Pt_2 6s	Pt_2 6p	C_{50} 2p	C_{51} 2p	H 1s	Ph_1* 2s,2p	C_{60} 2p	C_{61} 2p	Ph_2* 2s,2p	P 3s	P 3p	Et_{eff}* 2s,2p
48 (LUMO)	−5.42	1.1		0.1	0.3	0.1	2.5	20.9	3.6		67.4	0.2	0.2	0.3	0.1	0.4	1.8
49 (HOMO)	−5.78	0.2		1.9	0.3	0.4	0.8	3.5	1.3	0.2	1.9	2.9	3.1	82.5		0.1	0.8
1	147.10																
↑																	
4	84.71																
↑																	
31	11.36																
32	10.00																
↑																	
37	0.71																
38	−0.59	} unoccupied virtuals															
↑																	
47	−5.27																
↑																	
50	−6.04																
↑																	
82	−9.92	(major Pt contributions range from 5 to 34% in MO 50 through 100)															} occupied
↑																	
100	−11.26																
↑																	
153	−70.40																
154	−117.17																
155	−117.70																

[a] Ph_1* = "effective" phenyl attached to C_{61} (see text); Ph_2* = "effective" phenyl attached to C_{51}; Et_{eff}* = "effective" ethyl (see text).

Table IX. Maximum Percent Pt Character per Molecular Orbital[a] of 1a

MO (no.)	E, eV	Pt_1 5d	Pt_1 6s	Pt_1 6p	total Pt_1	Pt_2 5d	Pt_2 6s	Pt_2 6p	total Pt_2	grand total (Pt_1 + Pt_2)
51	−6.20			5.0	5.0			3.1	3.1	8.1
57	−7.97			3.7	3.7			4.6	4.6	8.3
63	−8.69		7.9		7.9				0.0	7.9
82	−9.92	20.3			20.3	9.0			9.0	29.3
84	−10.06	25.3			25.3	9.8			9.8	34.1
85	−10.15				0.0	21.7			21.7	21.7
86	−10.19				0.0	27.7			27.7	27.7
87	−10.30	21.2			21.2				0.0	21.2
88	−10.38				0.0	22.5			22.5	22.5
93	−10.67	20.2			20.2	10.4			10.4	30.6
95	−10.95	10.4			10.4	8.7	1.8		10.5	20.9

[a] Some of the MO in this sequence of levels (but not shown here) have Pt contributions from 5d orbitals between 5 and 17%.

Table X. Percent Ethylene, Acetylene, and Pt Orbital Contributions of 1a

MO (no.)	E, eV	C (50)	C (51)	C (60)	C (61)	Pt_1 5d	Pt_1 6s	Pt_1 6p	total Pt_1	Pt_2 5d	Pt_2 6s	Pt_2 6p	total Pt_2	grand totals ACN[a]	grand totals EtN[a]	grand totals Pt[a]
51	−6.20	8.8	6.0	4.6	1.4	0.9	0.9	5.1	6.9	0.8	1.7	3.2	5.7	6.0	14.8	12.6
53	−6.68	3.6	1.2	13.1	13.0	1.3		3.6	4.9	1.4	0.2	0.7	1.8	4.8	26.0	6.7
54	−6.80	0.8	0.2	33.4	36.8	1.3		0.6	1.9	0.2			0.2	70.2	1.0	2.1
55	−7.34	2.1	0.6	32.4	29.3	1.7		3.5	4.2	0.3			0.3	61.7	2.7	4.5
56	−7.69	12.1	6.8	2.6	2.7	1.8	1.5	0.6	3.9	7.3	0.9	5.7	13.9	5.3	18.9	17.8
58	−8.01	14.5	18.8	0.7	1.7	2.4	0.1	0.2	2.7	2.1		0.8	2.9	2.4	33.3	5.6
59	−8.02	7.8	9.9	0.8	2.7	1.0	0.1		1.1	1.2		0.5	1.7	3.5	17.7	2.8

[a] ACN = acetylene (C_{60}, C_{61}); ETN = ethylene (C_{50}, C_{51}); Pt = (Pt_1 + Pt_2).

tively, as shown in Table IX. It is also noted in Table IX that MO 85, 86, and 88 do not have a contribution from Pt(1), while moelcular orbital 87 does not have a contribution from Pt(2).

Those MO which contain both ethylene (C_{50}, C_{51}) and acetylene (C_{60}, C_{61}) contributions, plus some degree of Pt contribution, are presented in Table X. MO 54 and 55 are almost totally localized on the acetylene ligand. MO 51 and 56 are mainly delocalized over Pt–ethylene bonding, but molecular orbital 56 has in excess of three times more Pt(2) character than Pt(1) character.

Net atomic charges and pertinent interatomic bond populations are given in Table XI. The large negative charge on each of the Pt atoms (−1.07 and −1.18) is reminiscent of that found in the $Pt_2(P_2O_5H_2)_4^{4-}$ complex ion.[23] These charges and the large negative interatomic Pt(1)–Pt(2) bond population reflect the *absence* of a formal metal–metal bond in this complex. The nonnegligible population (0.355) in the Pt_1–acetylene (Pt_1–C_{60}) bond shows that the Pt valence electrons do interact with the acetylide ligand in this particular case. This is contrary to what is reported in earlier theoretical investigations of

Table XI. Some Atomic Charges and Interatomic Populations of 1a

atom	charge	bond	interatomic pop.[a]
Pt_1	−1.07	Pt_1–Pt_2	−0.467
Pt_2	−1.18	Pt_1–C_{50}	0.131
C_{50}	0.26	Pt_2–C_{50}	0.547
C_{51}	−0.09	C_{50}–C_{51}	1.075
H	0.007	C_{51}–H	0.633
C_{60}	0.03	Pt_1–C_{60}	0.355
C_{61}	−0.10	C_{60}–C_{61}	1.521
P_1	0.65	Pt_1–P_1	0.220
P_2	0.62	Pt_1–P_2	0.230
P_3	0.71	Pt_2–P_3	0.271
P_4	0.48	Pt_2–P_4	0.320

[a] 0.5 to <1.0, single bond type; 1.0 to <1.5, double bond type; 1.5 to <2.0, triple bond type. Negative values reflect repulsive bond polarity.

metal–acetylide bonds in general.[24]

A simple electrostatic approximation to the charge density on the vinylidene H atom (C_{51}–H) leads to an electron density of 0.19 e/Å^3. This is close to the 0.29 e/Å^3 deduced from electron density maps.[2]

Further refinements for attaining a more accurate computational model of this complex, as well as similar theoretical calculations of compounds **2**, **4**, and **10**, are currently underway and will be reported in detail elsewhere. We should mention that in an earlier qualitative description of the bonding in complex **1a** and in computations focussing on the mechanism of its formation, the authors mistakenly treated complex **1a** as an anion rather than as a cation.[25]

A preliminary study of the photochemical reactivity of some of these diplatinum compounds has been undertaken. Complex **1a** acts, under photolysis, as a catlayst for the conversion of isopropanol to acetone and molecular hydrogen. In a typical experiment, 0.01 mmol of **1a** is dissolved in 20 mL of methylene chloride containing 5 mL of 2-propanol. Photolysis of this solution at 16 °C using a 350-nm lamp (Rayonet reactor) produces an evolution of hydrogen gas (as monitored by a bubbler system) and the formation of acetone (as monitored by ^{1}H NMR). Hydrogen evolution begins upon irradiation of the system and occurs at a rate that increases slightly with time (presumably due to saturation of the solvent with hydrogen) and then decreases appreciably over a period of 4 h. After 8 h of irradiation, hydrogen evolution is too slow to be evident. Some amount of complex **1a** is recovered from the reaction solution along with a small amount of a yellow byproduct. ^{1}H NMR spectra of the reaction products clearly show the formation of a dinuclear platinum hydride complex. A hydride resonance consisting of a doublet of triplets is observed at δ −6.15 ppm with coupling constants of ca. 34 and 169 Hz. This byproduct does not contain the known mononuclear cation $[PtH(PEt_3)_3]^+$, which has a hydride resonance of similar pattern at δ −6.24 ppm with $^2J_{PH}$ coupling constants of only 15 and 156 Hz.[26] Over a total reaction time of 4 h, complex **1a** produces acetone and hydrogen with an average turnover number per hour of 15. In similar reactions, the Pt_2I compound **4** and the Pt_2Br_2 compound **10** also catalytically produce acetone and hydrogen from 2-propanol under irradiation with average turnover numbers per hour of 15 and 18, respectively. These average turnover numbers per hour are calculated from the total amount of acetone produced over a reaction period of 4 h. The respective total turnover numbers are, therefore, 60 and 72.

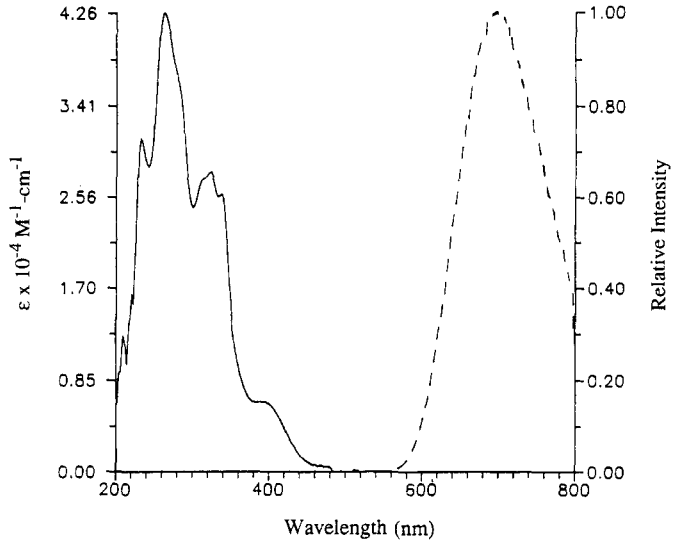

Figure 4. The absorption (solid line) and emission (dashed line) spectra of complex **2**. The absorption spectrum was recorded in CH_2Cl_2 solution at room temperature, while the normalized emission spectrum was recorded at 77 K in ethanol with excitation at 410 nm.

Complex **1a** does not react with methyl iodide at room temperature. However, **1a** reacts under photolysis with excess methyl iodide in acetone solution at 16 °C (Rayonet reactor) over a 4-h period to give a 33% yield of the Pt_2I compound **4** and a 25% yield of the Pt_2I_2 compound **11**. A similar reaction using irradiation from a Hanovia lamp source over an eight-hour period gives both products in yields of 26% and 10%, respectively. The remaining Pt is present as an unidentified yellow byproduct. Deposition of platinum metal is not evident in any of the above photochemical reactions.

We have undertaken a very preliminary study of the photophysics of the processes that occur when these diplatinum complexes absorb visible radiation. Complexes **1a** and **2** have similar absorption spectra in the wavelength range of 190–820 nm. Complex **1a** has a broad band of low intensity at 408 nm (ε = 6500 M^{-1} cm^{-1}) and a set of overlapping bands of greater intensity at 334 (ε = 20 000), 318 (ε = 23 000), 296 (ε = 25 200), 262 (ε = 35 100), and 232 nm (ε = 30 000 M^{-1} cm^{-1}). The corresponding absorption bands of complex **2** appear at 390 (ε = 6600), 338 (ε = 26 000), 324 (ε = 28 000), 264 (ε = 42 600), and 232 nm (ε = 31 600 M^{-1} cm^{-1}). Complex **2** also has weak tail absorption bands at 488 (ε = 470) and 626 nm (ε = 31 M^{-1} cm^{-1}).

Deaerated solutions of **1a** or **2** in methylene chloride do not give detectable emission spectra at room temperature upon excitation at either 400 or 296 nm. At 77 K, solutions of **1a** or **2** in 4:1 ethanol/methanol form a clear glass. Excitation of such a sample containing **1a** does not produce a detectable emission in the visible region. However, excitation of the sample containing complex **2** at 410 nm produces a red-orange luminescence that can be easily detected visually. This broad emission band has a λ_{max} at 696 nm. Φ ("optical" quantum yield) at 77 K is 0.010 ± 0.002. The emission spectrum of **2** along with its room-temperature absorption spectrum are shown in Figure 4. The emission spectrum is independent of excitation wavelength (410 or 488 nm).

The emission decay curves of **2** were nonexponential and could be fit with a sum of two exponentials. The lifetimes and relative contributions to the total steady-state emission

(24) (a) Kostic, N. M.; Fenske, R. F. *Organometallics* **1982**, *1*, 974–982. (b) Nast, R. *Coord. Chem. Rev.* **1982**, *47*, 89–124.
(25) Silvestre, J.; Hoffmann, R. *Helv. Chim. Acta* **1985**, *68*, 1461–1506.
(26) Church, M. J.; Mays, M. J. *J. Chem. Soc. A* **1968**, 3074–3078.

are 2.9 (0.44) and 0.7 μs (0.56). Assuming an average lifetime of 1.7 μs for the two components yields average values of $k_r = 6 \times 10^3\ s^{-1}$, $k_{nr} = 6 \times 10^5\ s^{-1}$, and $\tau_r = 170$ μs. The corresponding τ_r for $Pt_2(POP)_4^{4-}$ is 24 μs.

Discussion

Complex **1** reacts preferentially with halides, pseudohalides, and RS^- reagents to give the neutral, diplatinum, Pt_2X, compounds **2–8**. These complexes react with acid and an exogenous nucleophile, X^-, to give the neutral, diplatinum, Pt_2X_2, compounds **9–12**. Both types of dinuclear compounds contain bridging phenylethenylidene ligands. The propensity of complex **1** to react with ligands having an electronegative donor atom limits the extent of thermal reactivity for this compound. Neither the phenylethenylidene ligand nor the Pt–Pt bond of **1** exhibits the chemical reactivity anticipated for these functional groups.

Structural determinations of complexes **1a**, **2** (Pt_2Cl), **4** (Pt_2I), and **10** (Pt_2Br_2) reveal essentially normal structural features. The C=C bond distance within the μ-phenylethenylidene ligands ranges from 1.34 (2) to 1.38 (2) Å, and the C≡C bond distance in the terminal phenylacetylide ligands of **2** and **4** is 1.17 (2) Å. These distances represent normal C–C double and triple bond lengths. Structural data also indicate different coordination environments and different covalent radii for the two platinum atoms in each of these dinuclear complexes. The Pt–Pt distances of **1a**, **4**, **2**, and **10** are, respectively, 2.750 (2), 2.721 (1), 2.711 (1), and 2.685 (1) [average value] Å. These distances are within the normal range of Pt–Pt single bond distances,[27] although the trend of decreasing Pt–Pt distance with increasing electronegativity of the ligands donor atoms needs to be rationalized (vide infra). A particularly unusual structural feature of compounds **1a**, **2**, **4**, and **10** is that the principle coordination planes about Pt(1) and Pt(2) are nearly orthogonal and share only one vertex position (the donor atom of the μ-phenylethenylidene ligand). This geometrical arrangement may affect the nature of any Pt(1)–Pt(2) interaction.

New insights into the electronic structure and potential chemical reactivity of complex **1a** have been obtained from preliminary theoretical calculations. The salient results of these calculations are as follows: (1) the platinum atoms Pt(1) and Pt(2) bear large negative atomic charges of 1.07 and 1.18, respectively; (2) the negative value of −0.467 for the interatomic population of the Pt(1)–Pt(2) interaction reflects the absence of a formal metal–metal bond in this complex; and (3) the HOMO–LUMO energy separation is only 0.36 eV with the HOMO being centered primarily on the μ-phenylethenylidene ligand and with the LUMO being centered primarily on the phenyl ring of the terminal phenylacetylide ligand.

The large negative charge density on the Pt atoms effects a net electrostatic repulsive interaction between the two Pt atoms and presumably accounts for the overall antibonding interaction between the Pt atoms. These negative atomic charges should be reduced when a PEt_3 ligand or both a PEt_3 ligand and a phenylacetylide ligand are replaced by halide ligands or other ligands having electronegative donor atoms. This effect may account for the ligand preference exhibited by complex **1a**. As the electronegativity of the ligand set is increased, the Pt–Pt distance should decrease due to a decrease in the electrostatic repulsion between the two Pt atoms. This relationship between Pt–Pt distances and the electronegativity of the set of donor atoms explains the observed decrease in Pt–Pt distances along the series of compounds **1a**, **4**, **2**, and **10** (vide supra). Also, the location of the LUMO on the phenyl ring of the phenylacetylide ligand might explain the relatively low reactivity of **1a** toward nucleophilic attack assuming that frontier control of the reaction is operative.

Theoretical calculations of the $Pt_2(POP)_4^{4-}$ complex (using the same method as that reported here for compound **1a**) have revealed that the Pt atoms in this anionic complex also have an unusually high negative atomic charge (0.866) and that the Pt–Pt bonding interaction is very weak (8.05 kcal/mol).[23] A similarity in electronic structure between complex **1a** and $Pt_2(POP)_4^{4-}$ is not anticipated due to the structural differences between these two compounds. However, these theoretical results inspired us to investigate the potential photochemical reactivity of complex **1a** in analogy to that known for $Pt_2(POP)_4^{4-}$. The extensive chemistry and photophysical properties associated with the $Pt_2(POP)_4^{4-}$ species have been reviewed recently.[28]

Our preliminary study of the photochemistry and photophysical properties of complex **1a** and related compounds has yielded some promising results. The first example of C–H bond cleavage by $Pt_2(POP)_4^{4-}$ reported by Roundhill is the photochemical conversion of 2-propanol to acetone and molecular hydrogen.[29] Complexes **1a**, **4** (Pt_2I), and **10** (Pt_2Br_2) also act as photochemical catalysts in effecting this conversion. These compounds are photochemically active for reaction periods of at least 4 h and exhibit total average turnover numbers of 60–72. Although a detailed study of these reactions has not been completed, we have spectroscopic evidence that a dinuclear platinum hydride species is formed during these reactions. Presumably, an atom-transfer reaction similar to that proposed for $Pt_2(POP)_4^{4-}$ is occurring in these reactions, also.

Complex **1a** reacts with excess methyl iodide under photolysis to give the diplatinum iodide complexes **4** (Pt_2I) and **11** (Pt_2I_2) in good yields. Although the mechanism of this process is not known, an atom-transfer reaction has clearly occurred. Formation of **4** from **1a** requires the dissociation of one PEt_3 ligand from **1a**, and the formation of **11** from **1a** requires the loss of both a PEt_3 ligand and a phenylacetylide ligand from **1a**. The isolation of the diplatinum diiodide product **11** resembles the formation of $Pt_2(POP)_4Br_2^{4-}$ from the photochemical reaction of $Pt_2(POP)_4^{4-}$ with selected aryl bromides.[30]

The diplatinum complexes reported herein have a variety of types of states including ligand-localized, metal-centered, and metal-to-ligand charge-transfer (MLCT) states. This richness of states coupled with the low symmetry of the complexes makes an unambiguous assignment of all the optical transitions very difficult. However, a reasonable assignment of the absorption and the emission is possible. We first describe the possible excited states and then make assignments to the current spectra.

The dominant ligand transitions of **1a** and **2** would be spin-allowed π–π* transitions of the aromatic organic portion of the complex. Phenylacetylene has transitions at 272 (ε = 330), 248 (ε = 12 300), and 238 nm (ε = 13 800

(27) (a) Boag, N. M.; Browning, J.; Crocker, C.; Goggin, R. J.; Goodfellow, R. J.; Murray, N.; Spencer, J. L. *J. Chem. Res., Miniprint* **1978**, 2962–2983. (b) Balch, A. L. *Comments Inorg. Chem.* **1984**, *3*, 51–67.

(28) (a) Zipp, A. P. *Coord. Chem. Rev.* **1988**, *84*, 47–83. (b) Roundhill, D. M.; Gray, H. B.; Che, C.-M. *Acc. Chem. Res.* **1989**, *22*, 55–61. (c) See: Harvey, P. D.; Gray, H. B. *J. Am. Chem. Soc.* **1988**, *101*, 2145–2147 for related studies with Pt_2 d^{10}–d^{10} compounds and relevant references.

(29) Roundhill, D. M. *J. Am. Chem. Soc.* **1985**, *107*, 4354–4356.

(30) Roundhill, D. M.; Atherton, S. J. *Inorg. Chem.* **1986**, *25*, 4071–4072.

M^{-1} cm^{-1}). Thus, the bands below 250 nm in the complexes clearly involve at least some contribution from phenyl π–π^* transitions. Triethylphosphine has weak bands (50 M^{-1} cm^{-1} at 325 nm and 1500 M^{-1} cm^{-1} at 230 nm). None of these transitions would be visible in absorption spectra of **1a** and **2**. Thus, the spectra above 250 nm must be dominated by CT and metal-centered transitions.

The metal-centered transitions of similar d^8 complexes fall into two classes. In mononuclear complexes the crystal field splitting pushes the highest unoccupied d orbital above the lowest unoccupied p orbital; the lowest p orbital is the one perpendicular to the plane of the ligands p_z.[31] This results in the lowest metal-centered transition being d_{z^2}(metal)–p_z(metal). Since the p_z orbital can interact with the d orbitals of ligands, especially phosphines, there can also be mixing of metal p and ligand d orbitals. Thus, the extent of charge-transfer character in the d(metal)–p(metal) transition is the subject of debate. Dinuclear complexes formed from two square-planar units have the added complexity of interactions between the two p_z and between the two d_{z^2} metal orbitals, which results in bonding and antibonding p_z and d_{z^2} combinations. The lowest metal transition in such systems still appears to be a d(metal)–p_z(metal) transition, but the p state is the bonding combination arising from the two metal p_z orbitals.[33]

There can be two types of MLCT transitions. One involves promotion of a metal d electron to an aromatic ligand π^* orbital and the other to a phosphine d orbital. The phosphine MLCT transitions are of a symmetry to permit p_z interactions.

We turn now to the assignment of the spectra. The absorption spectra of **1a** and **2** are dominated in the 250–450 nm region by intense bands ($\epsilon > 3000$). These are much too intense to arise from aromatic ligand π–π^* transitions or phosphine transitions, and so they must arise from metal centered and CT transitions. These assignments are confirmed by the spectrum of the analogue of **1a** where the two phenyl groups have been replaced by hydrogen atoms.[33] Except for intensity changes the structure and energies remain largely unchanged. In particular, the 410 nm transition shifts to only 422 nm (shoulder, $\epsilon = 2800$ M^{-1} cm^{-1}). The similarity of the spectra of the non-phenyl-containing analogue of **1a** suggests that any CT transitions in this region must be to phosphine d orbitals and have negligible involvement of the π^* levels of the aromatic ligands.

The 410 and 390 nm absorption bands of **1a** and **2** are similar in intensity to the spin-allowed $d^8 \rightarrow d^7p^1$ absorptions of Rh(I) and Ir(I) mononuclear complexes with various phosphine and arsine ligands ($\epsilon \approx 1200$–5600 cm^{-1} M^{-1}).[34] Further, these transitions are largely insensitive to gross changes in the ligands, which is also true for the d–p transitions in the Rh(I) and Ir(I) systems. Thus, we assign the 390 and 410 nm absorption bands to a spin-allowed predominantly metal-centered $d^8 \rightarrow d^7p^1$ transition. A charge-transfer contribution to the d(Pt)–d(P) transition is also possible. We assign the weak absorption around 630 nm in **2** to the analogous spin-forbidden d–p transition.

There is the question of the involvement of Pt–Pt interactions. The two Pt atoms are close enough for interactions of p and d orbitals pointing toward each other as occurs in $Pt_2(POP)_4^{4-}$; however, a specific orbital description of such interactions is complicated by the low symmetry and unusual structure of these compounds. These d,p orbital interactions would raise the energy of the lowest occupied d orbital and lower the energy of the p orbital, thus reducing the transition energy over monomeric fragments. We suggest that metal–metal interactions are important in tuning the state energies of **1a** and **2**. The absorption spectrum of *trans*-bis(triethylphosphine)platinum(II) diacetylide is similar to that of **1a** and **2** below 350 nm but does not have the characteristic broad lower energy absorption band. This suggests that metal–metal interactions split the p level and drive the transition to lower energy for **1a** and **2**.

We turn to the luminescence. The radiative lifetime of 170 μs leaves no doubt that the emission arises from a spin-forbidden process. The very low emission energy precludes a ligand localized emission. Thus, the emission must be either metal centered or MLCT in character. The emission is strikingly similar to the d–p phosphorescences of Pt d^8 and d^{10} complexes.[35] The splitting between the spin-allowed d–p absorption transition and the emission of **2** is 11 300 cm^{-1}, which is similar to the shifts observed for the p–d phosphorescences of Rh(I) phosphines and arsines (8–11 kcm^{-1}).[34] Thus, we conclude that the emission is the spin-forbidden metal-centered p–d phosphorescence.

The very large splitting between the absorption and the emission indicates that there is large internuclear distortion in the excited state. Since excitation probably involves electron promotion into a bonding orbital between the two platinum centers, a large Pt–Pt internuclear distortion seems most likely.

The question arises as to why **1a** does not emit while **2** does. In view of the striking similarity of the lowest energy absorptions of these complexes, we suggest that the problem is not due to a change in basic excited-state pattern but is rather one of state energetics. The d–p absorption of **1a** is 1100 cm^{-1} lower in energy than for **2**. If both complexes have the same d–p singlet–triplet splitting, then the emission of **1a** would peak at 756 nm. This has two consequences that mitigate against our detecting the emission of **1a**. Our spectrofluorimeter is much less sensitive at 756 nm than at 696 nm, and the lower state energy would greatly reduce the luminescence efficiency of **1a** versus **2** because of more efficient radiationless deactivation. Thus, the failure to detect emission from **1a** is probably just a consequence of its lower yield and less accessible emission.

In relating the photophysical properties of these compounds to the observed photochemical reactivity, we believe that this excited state is the species responsible for the photochemistry exhibited by these compounds; however, further study is needed. It is also possible that intersystem crossing, like that observed in the photochemistry of $Pt_2(POP)_4^{4-}$, might be an important feature of the photochemistry of these diplatinum compounds. The photochemistry and photophysical properties associated with compounds **1a**, **2**, **4**, **10**, and **11** represent, to our knowledge, the most significant excited-state chemistry yet discovered for such complex *organometallic* molecules.[36]

On the basis of the discoveries discussed above in this preliminary report, we intend to study further the chemistry of these dinuclear complexes containing μ-alkenylidene ligands (and related compounds) with particular emphasis on characterizing the excited-state chemistry and

(31) Geoffroy, G. L.; Wrighton, M. S.; Hammond, G. S.; Gray, H. B. *J. Am. Chem. Soc.* **1974**, *96*, 3105–3108.
(32) Isci, H.; Mason, W. R. *Inorg. Chem.* **1985**, *24*, 1761–1765.
(33) Work in progress.
(34) Fordyce, W. A.; Crosby, G. A. *Inorg. Chem.* **1982**, *21*, 1455–1461.
(35) Caspar, J. V. *J. Am. Chem. Soc.* **1985**, *107*, 6718–6719.
(36) Lees, A. J. *Chem. Rev.* **1987**, *87*, 711–743.

photophysics of these molecules. A better understanding of the structural and electronic features of these molecules will also be pursued.

Conclusions

The preparation of several new diplatinum complexes containing μ-phenylethenylidene ligands is reported. X-ray structural determinations of three of these compounds confirm unambiguously the molecular structures of two new classes of diplatinum halide complexes. Theoretical calculations indicate that the electronic structure of these molecules might be similar to that found previously for $Pt_2(POP)_4^{4-}$. Study of the photochemistry and photophysical properties of several of these organometallic, diplatinum compounds reveals that selected compounds act as photochemical catalysts in the conversion of 2-propanol to acetone and molecular hydrogen and participate in halide to metal atom-transfer reactions under photolytic conditions. One complex emits a strong visually perceptible luminescence at 77 K when excited with radiation of 410 nm.

Acknowledgment. C.M.L. thanks the donors of the Petroleum Research Fund, administered by the American Chemical Society, for support of this research. A platinum metal loan from Johnson Matthey, Inc., is gratefully acknowledged. C.M.L. also thanks Professor D. M. Roundhill for a copy of a review article prior to publication. W.R.T. thanks the Graduate School of Vanderbilt University for a dissertation grant in support of this research. J.N.D. gratefully acknowledges support by the National Science Foundation (Grant CHE 86-00012) and also thanks Hewlett-Packard for the gift of the 8452A spectrophotometer and Henry Wilson for his kind assistance. P.G.L. thanks the Materials Laboratory of Wright Patterson Air Force Base for the use of their facilities for the X-ray data collection of compound **4**.

Registry No. **1a**, 106357-35-1; **1b**, 106357-37-3; **2**, 122236-05-9; **3**, 122236-06-0; **4**, 122236-07-1; **5** (thiocyanate), 122236-15-1; **5** (isothiocyanate), 122236-16-2; **6**, 122236-08-2; **7**, 122236-09-3; **8**, 122236-10-6; **9**, 122236-11-7; **10**, 122236-12-8; **11**, 122236-13-9; **12**, 122236-14-0; $NaSC_6Cl_5$, 22441-28-7; isopropyl mercaptan, 75-33-2; lithium isopropylthiolate, 16203-41-1; lithium thiophenolate, 2973-86-6; thiophenol, 108-98-5.

Supplementary Material Available: Tables of final atomic positional and thermal parameters, interatomic distances and angles, and selected least-squares planes data (30 pages); listings of final observed and calculated structure factors for the X-ray structures of compounds **2**, **4**, and **10** (98 pages). Ordering information is given on any current masthead page.

Formation of Carboxylate Complexes from the Reactions of CO_2 with Ethylene Complexes of Molybdenum and Tungsten. X-ray and Neutron Diffraction Studies

Rafael Alvarez,[1a] Ernesto Carmona,*[,1a] Agustín Galindo,[1a] Enrique Gutiérrez,[†,1b] José M. Marín,[†,1a] Angeles Monge,[†,1b] Manuel L. Poveda,[1a] Caridad Ruiz,[†,1b] and Jean M. Savariault[‡,1c]

Departamento de Química Inorgánica-Instituto de Ciencia de Materiales, Facultad de Química, Universidad de Sevilla-CSIC, Apartado 553, 41071 Sevilla, Spain, Instituto de Ciencia de Materiales, Sede D, CSIC, Serrano 113, 28006 Madrid, Spain, the Facultad de Ciencias Químicas, Universidad Complutense, 28040 Madrid, Spain, and the Laboratoire de Chimie de Coordination, CNRS, 31077 Toulouse Cedex, France

Received May 9, 1989

Carbon–carbon bond formation by coupling of ethylene with carbon dioxide on the coordination sphere of the metal center in the electron-rich complexes *trans*-$M(C_2H_4)_2(PMe_3)_4$ (M = Mo, **1**; M = W, **2**) can be effected under mild conditions by reactions of **1** and **2** with CO_2. These afford the binuclear hydrido acrylate derivatives $[MH(OOCCH{=}CH_2)(C_2H_4)(PMe_3)_2]_2$ (M = Mo, **3**; M = W, **4**), which contain bridging μ_2-η^3,η^1-acrylate ligands. Hydrogenation of **3** and **4** in the presence of PMe_3 provides the hydrido propionates $MoH(\eta^2\text{-}OOCCH_2CH_3)(PMe_3)_4$ (**5**) and $WH_3(\eta^1\text{-}OOCCH_2CH_3)(PMe_3)_4$ (**6**), but the direct reaction of **1** and **2** with a 1:1 mixture of CO_2/H_2 yields instead the hydrido carbonate derivatives $MH_2(\eta^2\text{-}CO_3)(PMe_3)_4$ (M = Mo, **7**; M = W, **8**). The hydrido allyl compounds $MH(\eta^3\text{-}C_3H_5)(PMe_3)_4$ (M = Mo, **9**; M = W, **10**), formed by sodium amalgam reduction of $MCl_4(PMe_3)_3$ under propylene, do not react with CO_2 with carbon–carbon bond formation but rather with reductive elimination of propylene and production of the adduct *trans*-$Mo(CO_2)_2(PMe_3)_4$ and various carbonate complexes. The crystal and molecular structures of **3**, **4**, and **6** have been determined by X-ray studies, and, in addition, a low-temperature (20 K) neutron diffraction analysis of **4** has been performed. **3** is monoclinic, $P2_1/n$, with a = 12.117 (8) Å, b = 15.072 (5) Å, c = 17.700 (5) Å, β = 102.18 (3)°, Z = 4, and R = 0.032, while **6** is monoclinic, $P2_1/c$, with a = 12.813 (2) Å, b = 8.903 (3) Å, c = 21.671 (3) Å, β = 88.62 (1)°, Z = 4, and R = 0.048. The crystal of **4** used for the neutron diffraction study is monoclinic, $P2_1/c$, with a = 14.23 (1) Å, b = 11.80 (1) Å, c = 20.58 (2) Å, β = 104.94 (6)°, Z = 4, and R = 0.034.

Carbon dioxide is an attractive and potentially useful C1 synthetic unit, but its scarce reactivity toward unsaturated organic fragments and its reluctance to undergo economically useful transformations promoted by transition metals constitute major drawbacks for its exploitation as a source of elemental carbon. Despite this inertia of carbon dioxide, many interesting reactions have been discovered in the last two decades,[2] and it is now widely

† To whom correspondence should be addressed on X-ray work.
‡ To whom correspondence should be addressed on neutron diffraction studies.

(1) (a) Universidad de Sevilla-CSIC. (b) Universidad de Madrid-CSIC. (c) Laboratoire de Chimie de Coordination, Toulouse.

0276-7333/89/2308-2430$01.50/0